UNIVERSITY OF CAMBRIDGE
Department of Engineering

In-path Soil Deformation under Moving Tyre

Author Name: T.L. Tse (Churchill)
Supervisor: Dr Stuart Haigh

Date: 29th May 2019

I hereby declare that, except where specifically indicated, the work submitted herein is my own original work.

Signed: ____________________________ Date: ______________

In-path Soil Deformation under Moving Tyre

T.L. Tse (Churchill)

Technical Abstract

Soil in pavements deforms due to traffic, which leads to the formation of ruts and potholes over time. This is because the existing pavement design methods are either empirical or mechanistic. Not all the factors that affect pavement deformation are taken into account in design. According to the 2019 Annual Local Authority Road Maintenance Survey (ALARM), 20% of the local roads in the UK are in poor structural condition, with less than 5 years of life remaining. To facilitate social and economic development, the government has allocated £28.8billion to invest in building new road networks and maintaining existing roads in the upcoming years. Therefore, it is critical to develop a better understanding of the way soil deforms so as to devise ways to repair defects and build more durable pavements. On the other hand, soil deformation due to the use of heavy machinery in farmlands also has huge implications on the yield of crops.

The accelerated pavement tester (APT) enables physical modelling of actual traffic conditions. A pavement structure was constructed in a concrete pit, with a window housed at the side to enable cameras to capture images during wheel travel. Images were then analysed by particle image velocimetry (PIV) to obtain information about soil movement. 3 sets of tests were carried out, each with a different pavement structure. Single layered and two-layered pavements were used to investigate the effectiveness of base course in reducing soil deformation. Surface layer was not used in any test. Within each test, 4 wheel loads were applied, each for 1 wheel cycle, to investigate the influence of load on soil deformation. The main focus of the study was on soil deformation due to an incremental wheel step.

Results show that the soil deformation mechanism in a single layered pavement structure consists of two flow zones, with the front zone wider than the rear. The mechanism was compared with the Prandtl mechanism for inclined load and another mechanism presented in previous literature. They were generally in good agreement. On the other hand, shearing in the flow zones causes volumetric dilation in the shallow region, resulting in reduction of shear strength after each wheel pass. A small degree of volumetric contraction happens at depth. The use of base course in two-layered pavement structure helps spread load over a greater area in the subgrade, which greatly reduces the amount of soil movement and changes the deformation mechanism. For both pavement structures, soil displacement increases linearly with load. Depth of flow zones also increases with wheel load but to a lesser extent in a two-layered pavement.

To determine whether the existing layered elastic theory is suitable for characterising deformation due to pavement traffic, soil displacement throughout 1 wheel pass was evaluated and compared with the theory. For a single-layered pavement, dilation near the

surface implies that the model should not be used as it predicts downward movement throughout the pavement by treating the moving wheel as a static load. At depth, there is good agreement between the experimental results and the theory. As for a two-layered pavement, the theory overestimates soil displacement but results are conservative.

This project looks into soil deformation due to pavement traffic at a fundamental level. Further work is needed to develop a comprehensive understanding of the problem. This includes running greater number of wheel cycles and modifying the existing experimental setup to better model the actual pavement structures found in different places and the operation of drive wheels in vehicles.

Contents

1 Introduction

Traffic causes soil deformation in pavements, affecting their serviceability. Ruts form over time as permanent deformation accumulates with repeated load cycles. In the event of rain, ruts trap water on the wheel path and prevent it from draining to the sides of the road, leading to hydroplaning. Pothole is another common defect seen on pavements, which is formed as water seeps into the subsurface and weakens the soil underneath. Over time, the surface layer cracks due to fatigue failure. These defects increase the risk of car accidents due to the loss of braking and steering control. In addition, they also pose danger to other road users such as cyclists as it is often difficult for them to steer away from ruts and potholes, especially when it is dark at night. Additional cost is also required for owners to repair their cars and bikes in the event of accidents.

According to the 2019 Annual Local Authority Road Maintenance Survey (ALARM), 20% of the local roads in UK are in poor structural condition, with less than 5 years of life remaining [3]. Statistics from the Department for Transport show that the number of car accidents happened in Scotland due to poor road environment was 5 times that due to drink driving from the period of 2010 to 2018 [4]. This highlights the severity of poor pavement conditions. With rapid economic and social development, the government allocated £28.8billion to the National Roads Fund between 2020 and 2025 to invest in new major road networks and local roads in Budget 2018 [2]. £420million was allocated to road maintenance between 2018 and 2019. There is an urgent need to improve the existing pavement design to build pavements that are more durable. It is also vital to devise means to repair worn out pavements effectively.

On the other hand, soil deformation due to the use of heavy machinery on agricultural lands is also a topic of great concern. Unlike pavements, farmlands are not engineered and are subjected to higher loads, thus greater soil compaction occurs. Heavy compaction restricts root penetration in soil and also limits water and air infiltration [19], which adversely affects the yield of crops. To increase productivity, heavier vehicles are developed in recent years. A better understanding of soil-wheel interaction would possibly help engineers develop new farmland structure that is more robust against soil compaction.

2 Aims

This project aims at investigating in-path soil deformation under moving tyre by physical modelling. The focus is mainly on pavement deformation, but results can also be extended to apply to agricultural land. The objectives of this project are:

- To understand the in-path soil deformation mechanism in single layered and two-layered pavements.
- To understand the influence of loads and travel repetition on soil deformation.
- To assess the effectiveness of base course layer in reducing soil deformation.
- To compare experimental results with existing layered elastic model in predicting soil movement.

3 Literature Review

3.1 Pavement Design

Pavements in urban area have layered structures to withstand traffic loads. The outline of a typical structure is shown in Figure 1 but details vary according to its use and location. The surface layer serves as a barrier to water and provides skidding resistance while the base course is usually made up of unbound granular materials such as gravels, which acts as the main structural layer to distribute the surface stress to reduce the stress and strain in lower layers. The bottom subgrade layer consists of fine natural soil found in the area. Note that the surface layer and sub-base layer are not used in this project for simplicity.

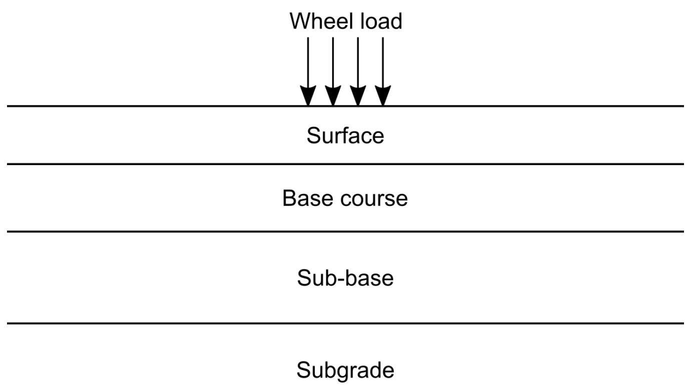

Figure 1: Pavement structure [8]

The commonly used pavement design method in the UK is set out by the Highways Agency, which is known as the CBR method [8][9]. The thickness of each layer is determined from its resilient modulus E, which is calculated empirically using formula (1).

This method has its shortcomings as it relates an elastic property E with the California Bearing Ratio CBR, which is a measure of shear strength. It is known that the relationship between E and CBR is also dependent on other factors including soil type and stress level. Moreover, this method fails to capture the irrecoverable strain response of soil under cyclic wheel loads, which is the primary cause of pavement failure. It simply aims to prevent shear failure in the subgrade for pavement structure with thin surface layer.

$$E = 17.6CBR^{0.64}MPa \tag{1}$$

On the other hand, mechanistic design method has been developed by treating pavement as a layered elastic system. Burmister [11] derived equations for stress and displacement in two-layered pavement based on the layered elastic theory. Wheel was treated as a stationary circular contact patch with load acting vertically downwards. The interface between the top and bottom layers was assumed to be either frictionless or fully frictional. Soil was characterised by Young's Modulus E and Poisson's ratio ν. These assumptions are ideal and oversimplifies the pavement deformation problem. Despite soil has non-linear stress strain relationship, E was taken as constant in calculations. Besides, the derivation treated pavement traffic as a static problem, which is not the case in reality since wheel load is transient and cyclic.

The above methods do not take into account of the dynamic nature of pavement traffic and also fails to capture all the parameters that affect pavement deformation in design. This project attempts to improve the understanding in how pavement responds to traffic loads, so as to devise better design methods.

3.2 Soil Stress and Deformation

Traffic induces cyclic vertical, horizontal and shear stresses on the soil beneath (Figure 2). Both vertical and horizontal stresses increase as the tyre approaches and decrease as it leaves. Shear stress reverses direction when the wheel is directly above any given soil element. This leads to principal stress axis rotation (PSAR).

Soil deformation under a moving tyre can be classified into two categories: resilient deformation and permanent deformation. The former is concerned with recoverable strain that occurs during each load cycle, which can possibly lead to fatigue cracking of surface layer in the long term. Permanent deformation is minimal in each cycle but accumulates with travel repetition and causes surface rutting, which affects the serviceability of pavements. Rutting profile is complex and is discussed in more detail in Section 3.5. This project focuses on investigating permanent soil deformation.

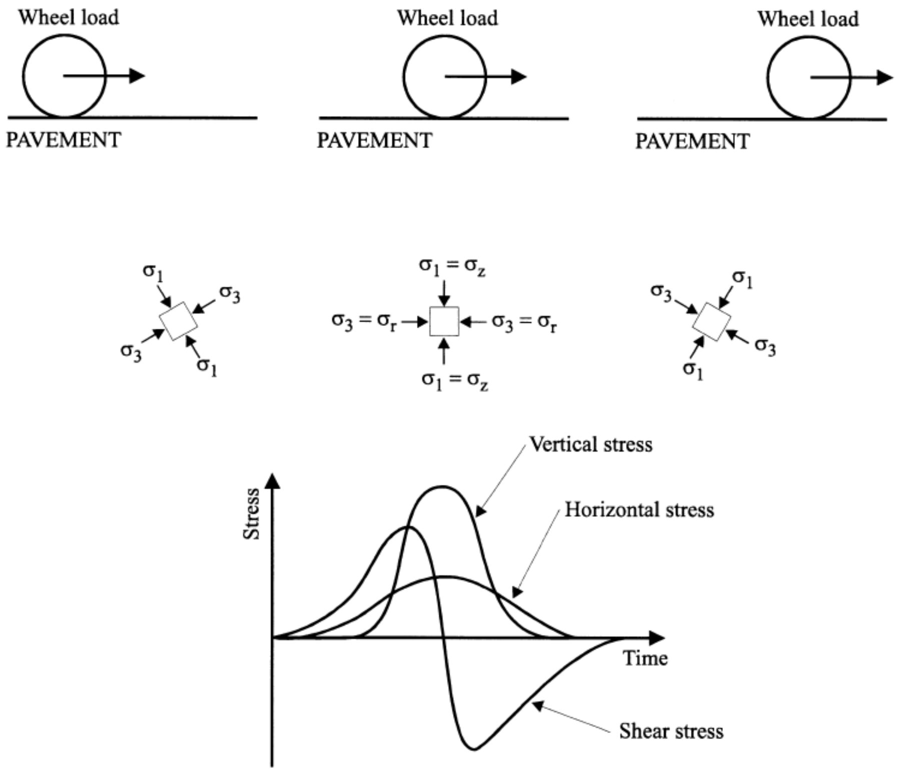

Figure 2: Stresses in pavement [15]

3.3 Laboratory Element Tests

Early research focused on using laboratory element tests to characterise soil behaviour under moving wheel load. Repeated load triaxial (RLT) test was initially used to understand how permanent axial strain in soil varies with the number of load cycles. However, this test does not model the shear stress reversal phenomenon and thus, underestimates permanent deformation in pavements. The multi-ring shear apparatus (MMRS) [12] developed in later years enables application of cyclic torsional shear and vertical stress, which simulates actual traffic conditions.

Figure 3 shows the significance of PSAR in plastic deformation of soil. The MMRS moving wheel load (MWL) test, which simulates PSAR, records considerably greater permanent axial strain than the single point load (SPL) test. Further studies suggested that this is due to the anisotropy of soil, which causes shear resistance to reduce when the mobilised plane coincides with the bedding plane during PSAR [17]. This suggests that the RLT, which is similar to the SPL test, is not suitable for characterising soil-wheel interaction. On the other hand, the use of MMRS gave a reasonably good estimate of the actual pavement permanent strain when compared with results from model test. Permanent deformation is also dependent on factors including water content, shear stress amplitude, load frequency and density [12][14]. For both MMRS and RLT tests, it was found that the long term soil deformation behaviour is dependent on stress ratio [15].

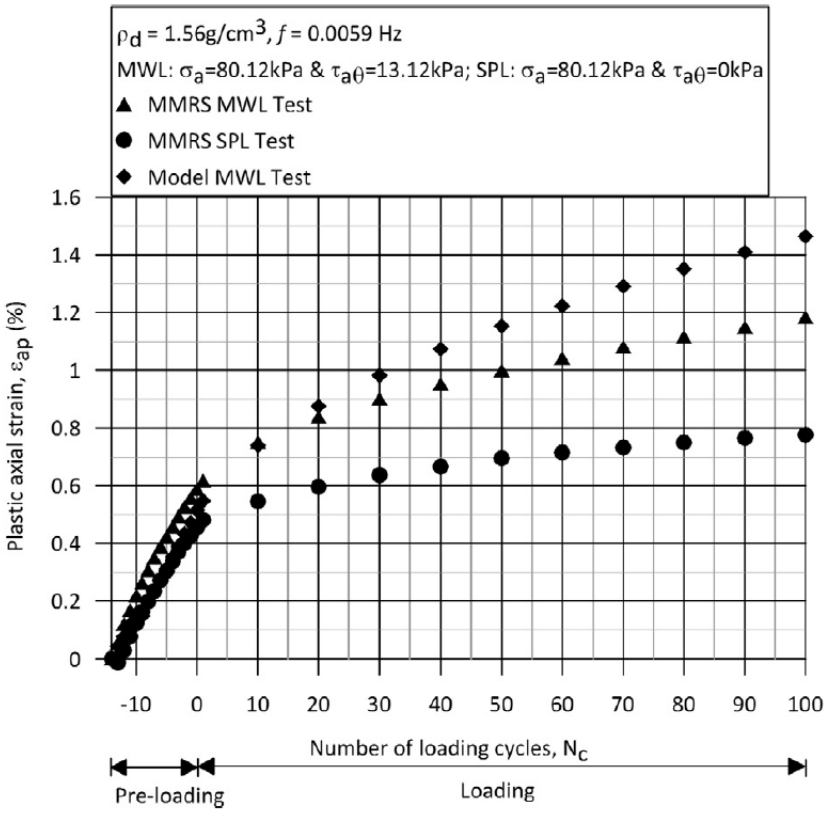

Figure 3: Laboratory element test [12]

Permanent strain settles to a constant value at low shear stress ratio. As for high shear stress ratio, progressive deformation occurs until failure and this transition happens at the shakedown limit.

Although the MMRS test is able to simulate stress induced by traffic, its significance remains limited as it only focuses on one parameter: permanent axial strain. It fails to capture the way soil particles move. This project makes use of cameras and PIV technique to fully capture the deformation mechanism.

3.4 Soil Displacement Trajectory

Wheel travel test [21][22] was carried out by pulling a rigid wheel in a soil bin with sandy layer. PIV was then used to analyse the soil displacement trajectory under different test conditions. Results show that each soil particle moves in a spiral path (Figure 4) in each wheel travel. Soil particle in front of the wheel moves forward and upwards. As the wheel approaches, the particle moves forward and downwards. Its horizontal direction then slowly changes to backwards. The particle reaches its lowest position when the wheel is directly above it. As the wheel passes, the particle moves rearward and upwards.

The exact shape and size of the trajectory is dependent on many factors. With greater slip ratio, particles tend to displace upwards and rearward throughout the wheel cycle.

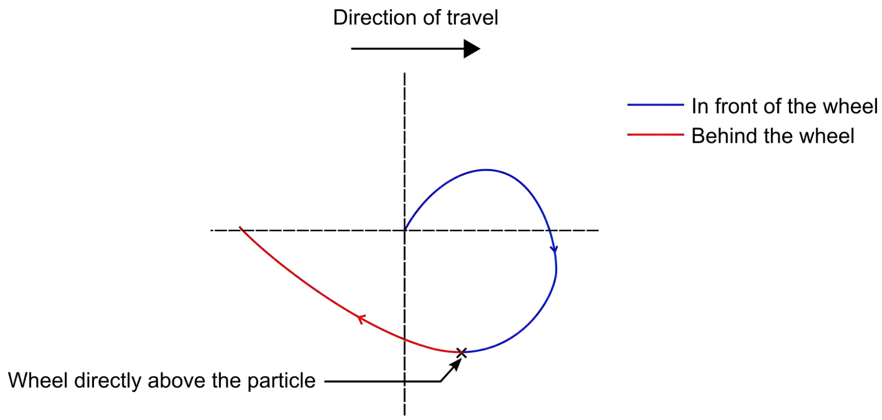

Figure 4: Soil particle trajectory

Also, the area of the trajectory tends to decrease exponentially with depth. At small slip ratio, soil movement at surface is not affected by travel repetition but the trajectory size at depth was found to decrease exponentially with travel. Overall, soil movement results in increase in voids ratio in shallow layers and decrease in deeper layers.

The above test tracked how individual soil particles move at several locations of interest, but did not capture the entire picture. Also, analysis was mainly done qualitatively and the wheel load used was small (0.2kN), which is not representative of the range of loads that is anticipated on pavements. As the study was mainly focused on soil deformation in natural terrain, layered pavement structure was not used in the setup. Thus, it is necessary to carry out experiment that replicates the actual pavement structure and loading conditions to understand the overall deformation mechanism.

3.5 Previous Research on Deformation Mechanism

Rutting occurs in soil under moving tyre and its deformation field is three-dimensional (Figure 5). In the transverse direction, there is soil upheaval along both sides of the wheel, which represents two flow zones. Wheel can be treated as a shallow foundation and sliding block mechanisms can be used to characterise the deformation behaviour despite it was developed for monotonic loading [7]. On the other hand, deformation mechanism in the longitudinal direction is more complex and is the focus of this project. Limited research has been done in this area and the mechanisms proposed by previous literatures are described briefly below.

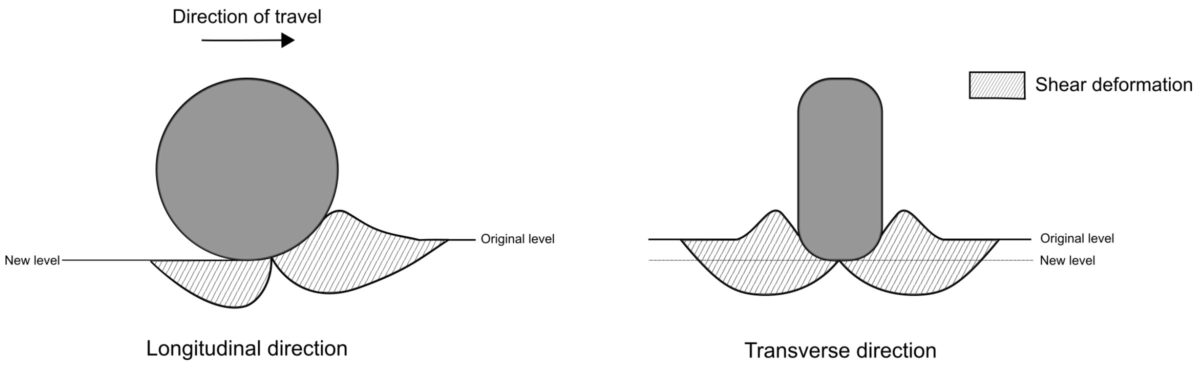

Figure 5: Rutting profile

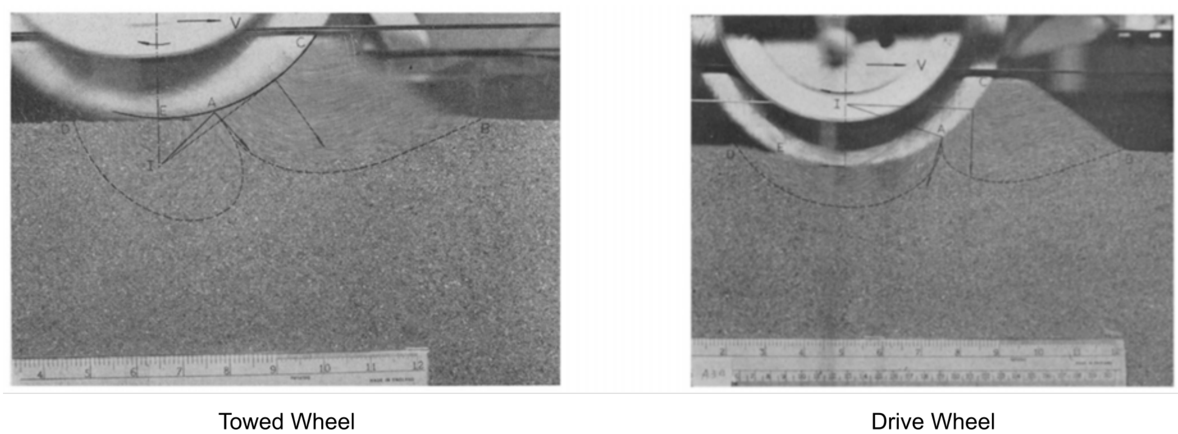

Figure 6: Flow pattern in dry sand (load = 0.56kN, slip = 28% and 37%)[26]

3.5.1 Soil-Wheel Interaction Model Proposed by Wong

Studies were conducted by Wong [25][26] using photographic methods to identify flow zones when wheel travelled in a soil bin. Dry sand was used in the experiment to simulate conditions in natural terrain. As the wheel travels, it shoves some soil forward, forming a step in front of the wheel. It was observed that the front and back flow zones were not identical (Figure 6). The front zone is shallower, wider and intersects the surface at $\mu = 45° - \frac{\phi}{2}$, where ϕ is the friction angle. It can also be seen that the shapes of the flow zones are slightly different for towed wheel and drive wheel because of the difference in instantaneous centre of wheel rotation. The shape also depends on the type of soil, i.e. sand or clay. For sand, each flow zone is bounded by a logarithmic spiral with a straight line whereas for clay, it is bounded by a circular arc with a straight line extending to the surface.

Stress analysis [27] showed that the transition point where the two zones meet coincides with the point of maximum radial stress and shear stress reversal. As seen in Figure 7, the distribution of radial stress is almost symmetric. Therefore, it can be deduced that the line joining the wheel centre and the transition point is in the same direction as

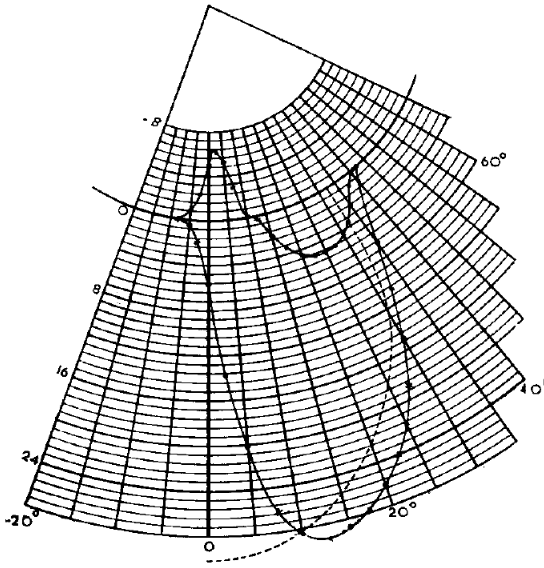

Figure 7: Distribution of radial and shear stress on sand for towed wheel (slip ratio = 44.5%) [20]

the resultant wheel force. It was also found that the location of the transition point is dependent on slip ratio.

The above study identified flow zones by looking for the boundaries between fine grains of stationary soil and streaks of moving soil on the image captured by long film exposure. Thus, the accuracy of this method is questionable. Moreover, the experiment did not look into the extent of soil movement within the flow zones and was conducted at low loads which is not comparable with loads from vehicles. The soil structure used in this study is also different from engineered pavements.

3.5.2 Numerical and Analytical Models

Previous study by Hambleton [13] on terramechanics in natural terrain involved simulating the rolling process of towed wheel three-dimensionally using finite element code ABAQUS to produce a displacement vector field for an incremental wheel step. To ensure computational stability, cohesion had to be introduced into the model regardless of the soil type. Small-scale experiment was also conducted in soil bin to track soil movement using PIV so as to evaluate the performance of the numerical model. Figure 8 shows that numerical modelling failed to capture movement in the rear flow zone and the avalanching of soil pile formed in front of the wheel. This is because the model computed tensile isotropic stress in those areas, when in reality soil does not sustain tensile force. This shows that the use of numerical model in understanding soil deformation is limited as it is impossible to fully characterise the soil properties when formulating the model.

On the other hand, Hambleton proposed analytical models to approximate soil-wheel interaction. Knowing that the wheel force on soil is inclined at an angle, inclined force

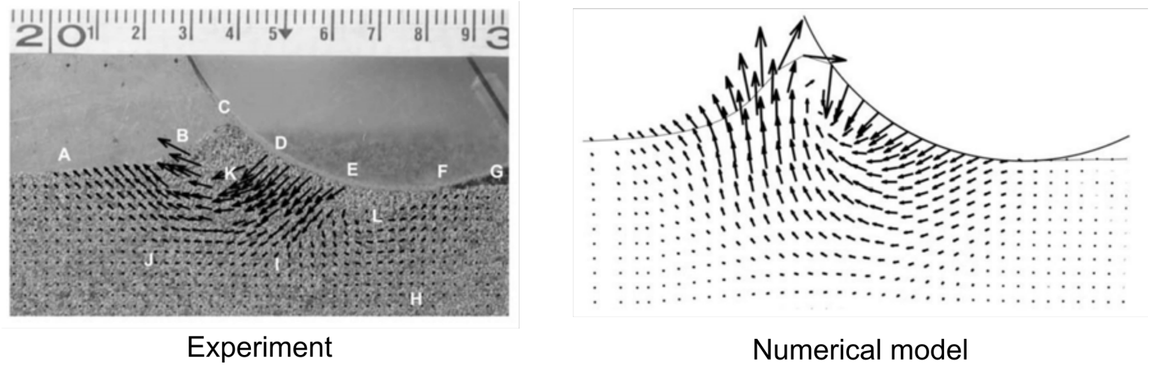

Figure 8: Incremental displacement field from experiment and numerical model [13]

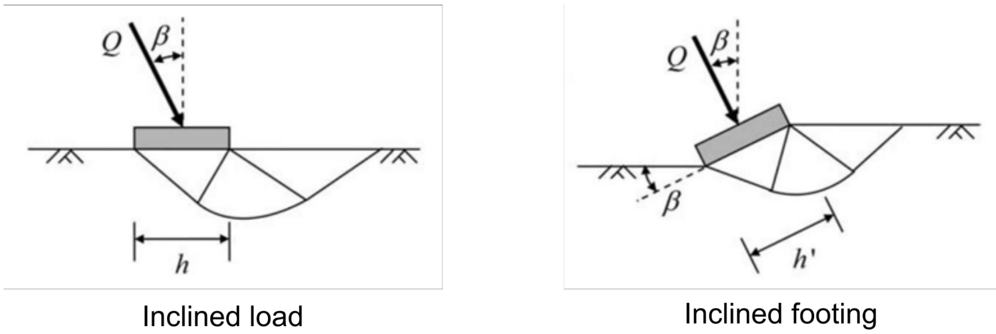

Figure 9: Proposed analytical models [13]

model and inclined footing model (Figure 9) were proposed by treating the contact patch as a shallow foundation. Relationship between load and wheel sinkage was established by using the Terzaghi-Meyerhof formula [16] for bearing capacity with appropriate factors. It was found that prediction using the inclined footing model is closer to experimental results, in particular for frictional material. However, wheel sinkage is only one of the many parameters that characterise soil deformation. Attempts were not made to verify how well these models predict the deformation mechanism.

3.5.3 Other Studies

Recent study on soil-wheel interaction in terramechanics involved using advanced image processing techniques [18] to provide details of soil movement in a soil bin test. The research focused on loose granular soil to simulate environment on planetary bodies. Results gave an qualitative indication of the direction and magnitudes of soil velocity within flows zones (Figure 10). However, results are not entirely comparable to what would be observed in actual pavement where soil is usually well compacted and has a layered structure. Thus, the use of the APT and PIV analysis would help simulate actual traffic on pavements and perform quantitative measurement of soil movement.

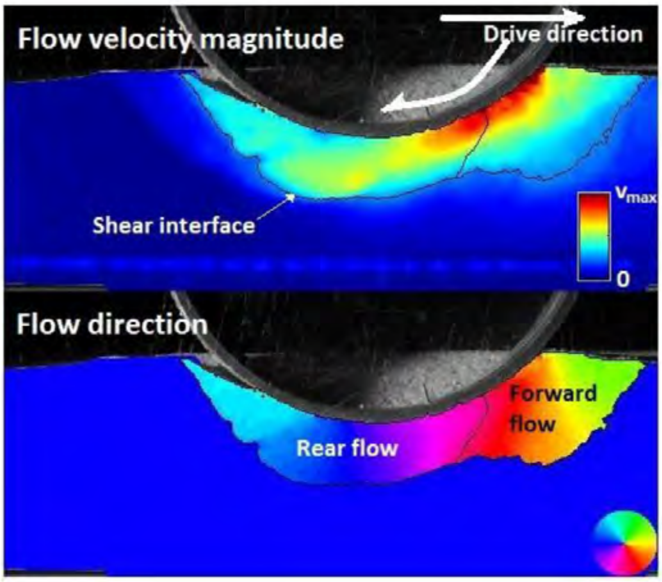

Figure 10: Shear interface imaging plot in loose granular soil beneath a drive wheel (load = 0.1kN, slip ratio = 20%) [18]

4 Theory and Experiment

4.1 Accelerated Pavement Tester (APT)

The accelerated pavement tester (APT) [5] enables physical modelling of actual pavement traffic conditions in a laboratory environment. It was originally developed to study subsurface deformation in airfield pavement under aircraft loading. The APT (Figure 11) travels on a pavement structure constructed in a concrete pit. Soil movement is captured through a window housed at the side of the pit by using cameras and images are analysed using particle image velocimetry (PIV).

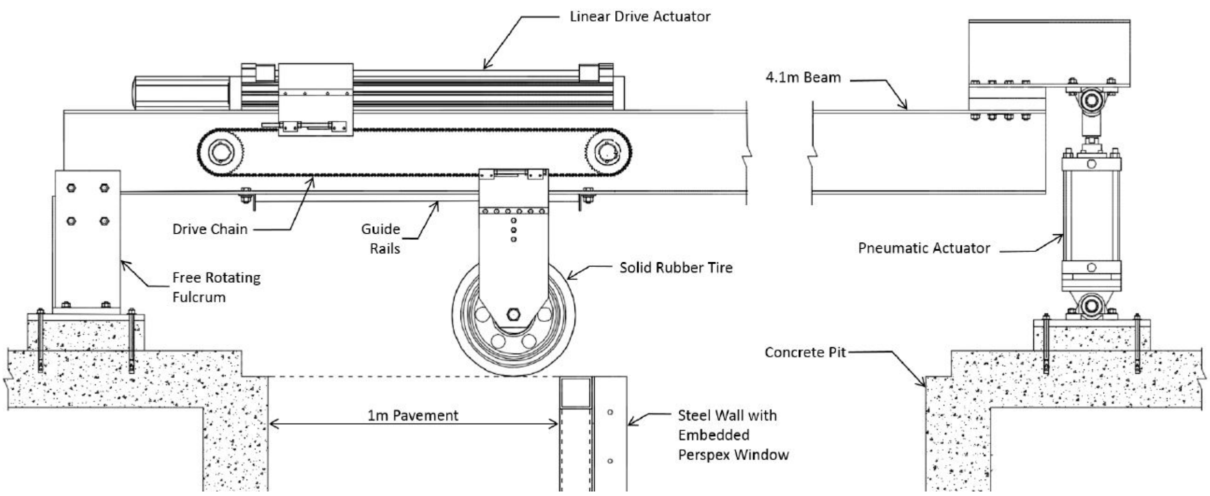

Figure 11: Side view of the accelerated pavement tester (APT) [6]

The tyre is towed by a drive actuator. Load is applied onto the rubber tyre via a lever arm mechanism between the pneumatic actuator and the fulcrum. It is capable of applying loads from 2.5kN up to 38.0kN. A total of 8 strain gauges are mounted on the two tyre supporting plates to measure the actual load on the pavement. The measurements are averaged to take into account of the possibility of uneven loading due to unlevel surface. Travelling speed and load can be controlled via a digital system. The strain gauge readings, tyre position and inclination of beam are recorded continuously and a feedback system is used to perform correction to maintain constant load and speed throughout wheel travel.

The performance of the APT was monitored during tests and Figure 12 shows that there was generally a constant offset of 0.70kN between the demanded load and the measured load. This is probably because loads used in this project were near the lower end of the APT loading range, where the relationship between the actuator pressure and strain gauges is not quite linear. The experiment had two loading scenarios, running on either base course or subgrade layer. The load vs time graph in Figure 13 is only plotted for 1 load as the APT behaved in the same manner regardless of loads. In general, it can be seen that the load on the pavement was fairly constant throughout each wheel pass. The subgrade layer curve is more spiky because the surface was less smooth. In particular, high peaks can be seen at the end of the cycle. This is caused by soil piling up at the front due to the shoving, which stopped the tyre from moving forward and the control then applied more force, resulting in a jump in the curve. Overall, the feedback mechanism worked quite well.

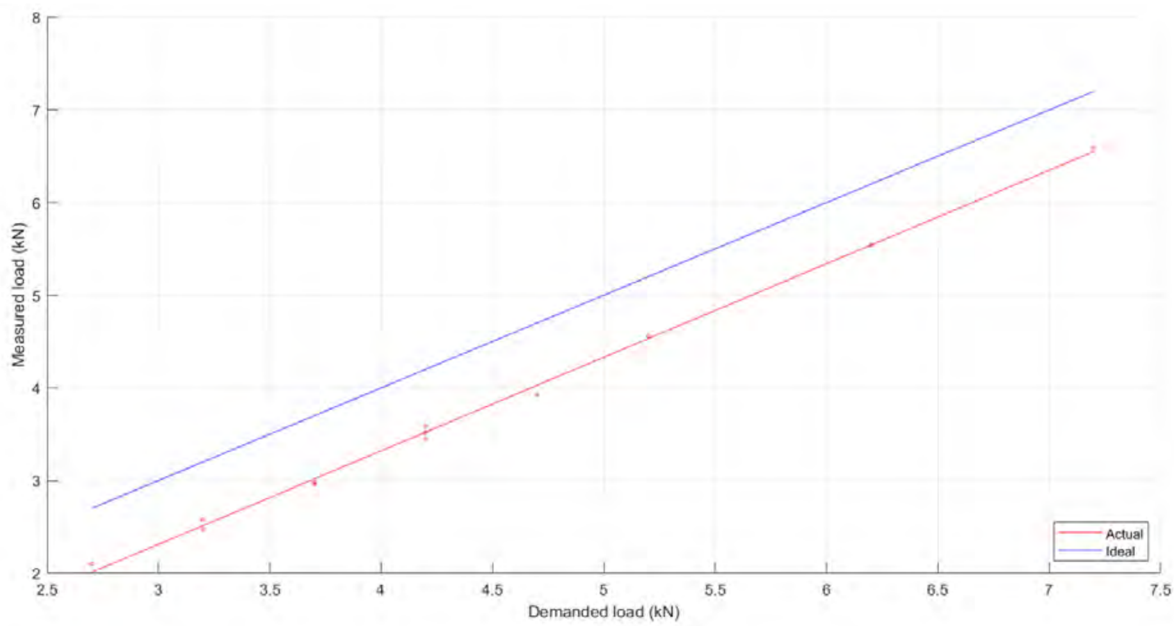

Figure 12: Demanded load vs measured load graph

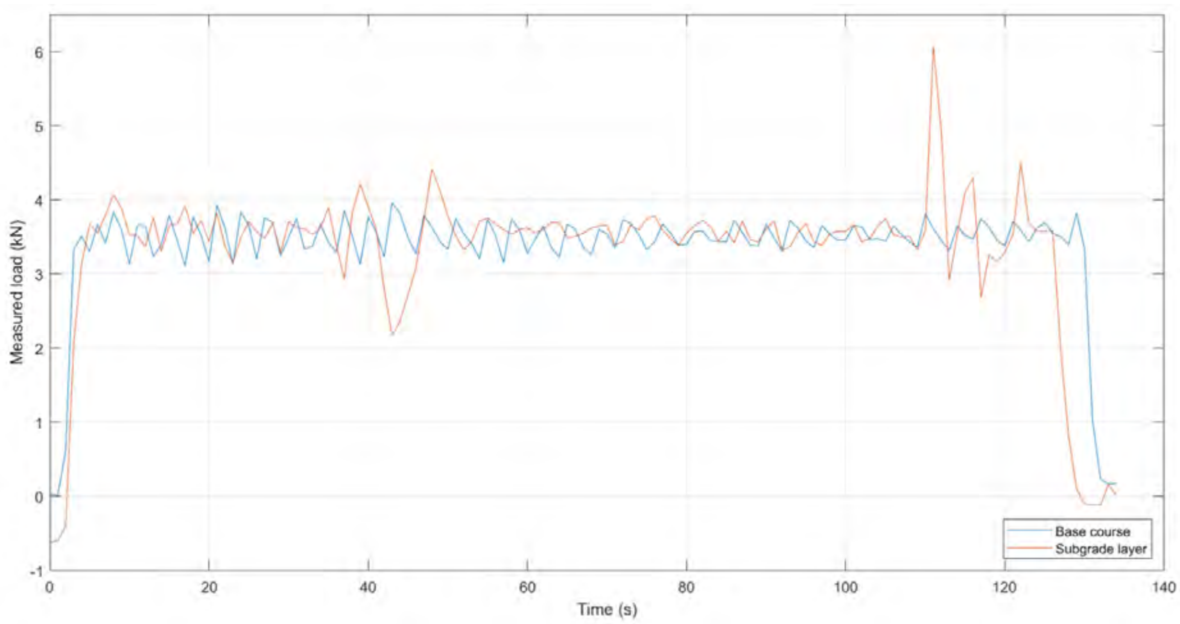

Figure 13: Load vs time graph (load = 3.50kN)

4.2 Experimental Setup

A pavement structure was constructed in a concrete pit with dimensions 1000mm × 800mm × 860mm. To reduce frictional boundary effects at the side walls, the pit was lined with geomembrane, which helped reduce the shear stress by 95% [5]. The layout of the experimental setup is shown in Figure 14. Details of the soil used are displayed in Table 1. The experimental setup process is outlined below:

1. Soil sample was taken and put into the oven overnight to obtain the water content by measuring weight. Water was added to the soil and mixed using a cement mixer to achieve optimum water content if necessary.

2. The bottom 500mm was constructed in layers of about 100mm. The mass of soil required was calculated before lifts. Each layer was levelled using a spirit level.

3. Each layer was compacted using a plate compactor to optimum modified Proctor values. The depth of soil surface from ground was then measured to give an indication of whether further compaction was needed.

4. A 100mm thick Perspex window was fitted into place when the level reached -500mm. Wooden planks were used to prevent movement of the window due to soil pressure. Control points were marked on the window to help image-object space calibration when processing data.

5. The remaining 500mm layer was constructed in the same way as before. The type of soil used in the top 140mm depended on the test to be carried out. Precise

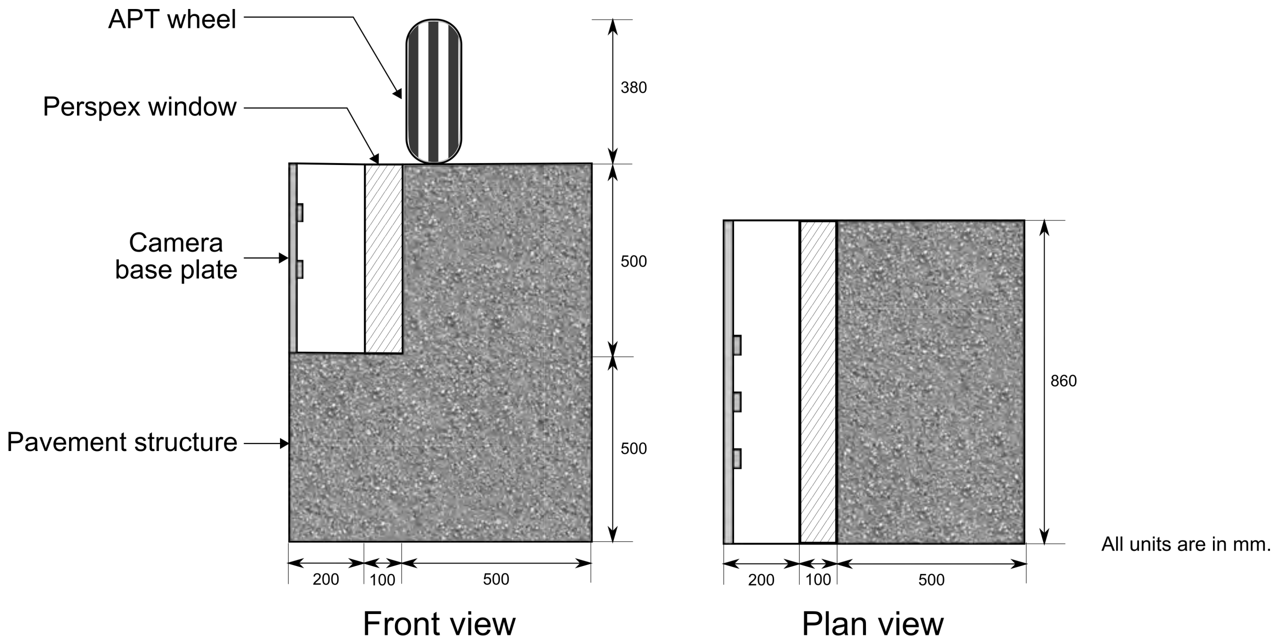

Figure 14: Soil pit layout

	Subgrade	Base course
Soil type	Kazakhstan medium silt-sand (KW15)	Limestone aggregate
Mean particle size D_{50} (mm)	0.30	5.60
Optimum water content w_{opt} (%)	9.8	12.8
Dry unit weight γ_d (kN/m^3)	19.0	16.1
Cohesion (kPa)	7.4	0
Friction angle ϕ_{crit} (°)	31	38
Young's modulus E (MPa)	13.16	19.33
Poisson's ratio	0.3	0.2

Table 1: Soil properties [5]

levelling was required at the topmost layer to provide a smooth surface for the APT to operate on.

6. Six Raspberry-Pi cameras were mounted on a steel base plate fixed on the side of the pit to capture the soil profile through the window. The cameras were connected to the computer system, where the user could trigger the cameras to start capturing images simultaneously.

7. An LED light was placed at the top of the window to ensure that the images captured were well illuminated.

8. The APT was moved into place ready for testing.

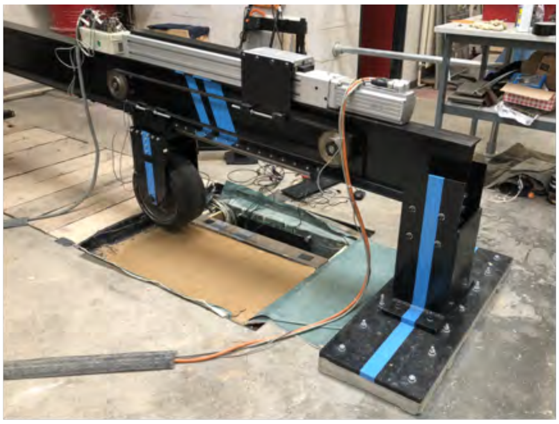

Side view (with APT)

Subgrade layer

Base course

Plan view (without APT)

Figure 15: Completed experimental setup

4.3 Test Overview

3 sets of tests were carried out, each with a different experimental set up as illustrated in Figure 16. The pavement structure was varied to investigate the influence of base course thickness on soil deformation. Wheel loads were set by taking into account of the actual traffic on pavements. From manufacturer tyre specifications [1], the maximum pressure of a load range D (8-ply rating) light truck tyre is given as 65psi. The APT reference load was chosen such that its tyre pressure would be close to 65psi. Figure 17 was used to calculate the tyre pressure based on the contact patch size and tyre load. 3.2kN was then chosen to be the reference demanded load to be applied on the pavement with a pressure of 62psi. Note that from this Section onwards, all loads refer to the measured loads.

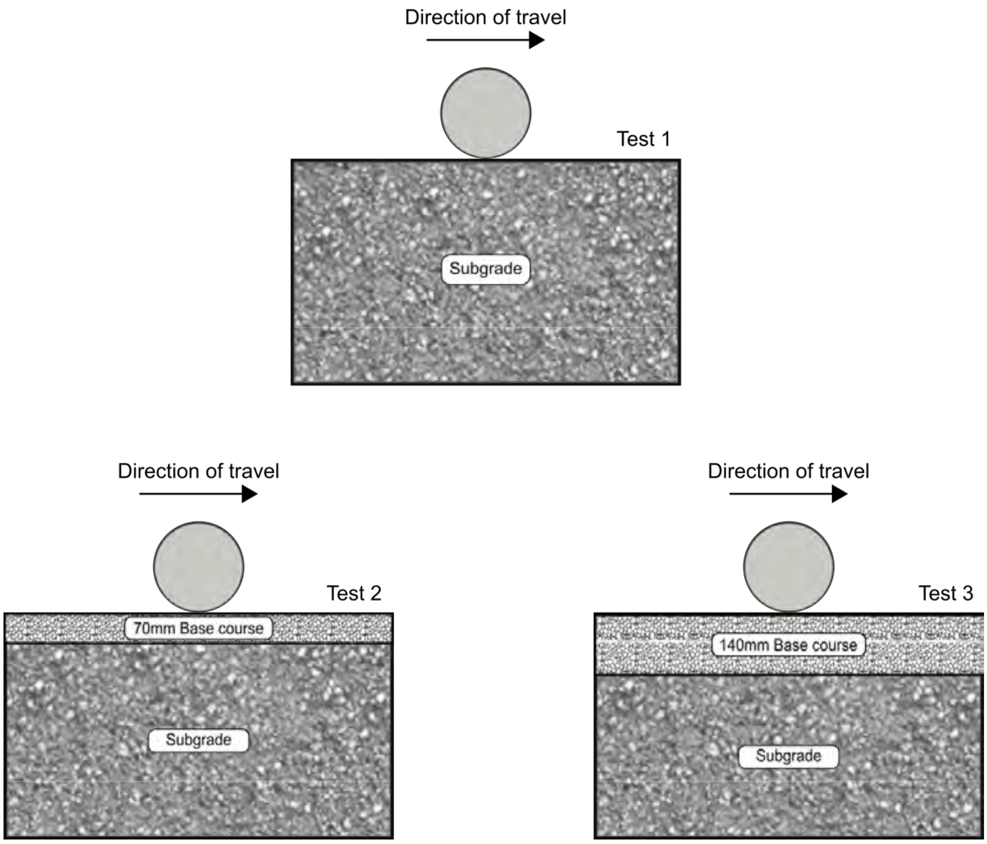

Figure 16: Side view of the top 500mm of the experimental setup

4 loads were used for each test to investigate the influence of load on soil deformation. Details are displayed in Table 2. It can be seen that each test had a different set of loading range, increasing from test 1 to test 3. With thicker base course, it is expected that the soil would deform less. Therefore, greater loads were applied for test 2 and test 3 to ensure that soil movement could be tracked by PIV. The reason why the loads in test 1 was kept low is because it was observed during preliminary test that severe rutting occurs at loads above 3.50kN, which would obstruct wheel movement. To ensure that comparison across the 3 tests is possible, a common load was used across tests, which is 3.50kN.

4.4 Experimental Method

The following steps were undertaken to complete each test:

1. The LED light was turned on and a test on the cameras was carried out to check the image quality. If it was not up to standard, changes had to be made on the focus of the cameras or the setup of the LED.

2. The pressure valve for the pneumatic actuator was turned on.

3. The load and travelling speed were inputted into the control system.

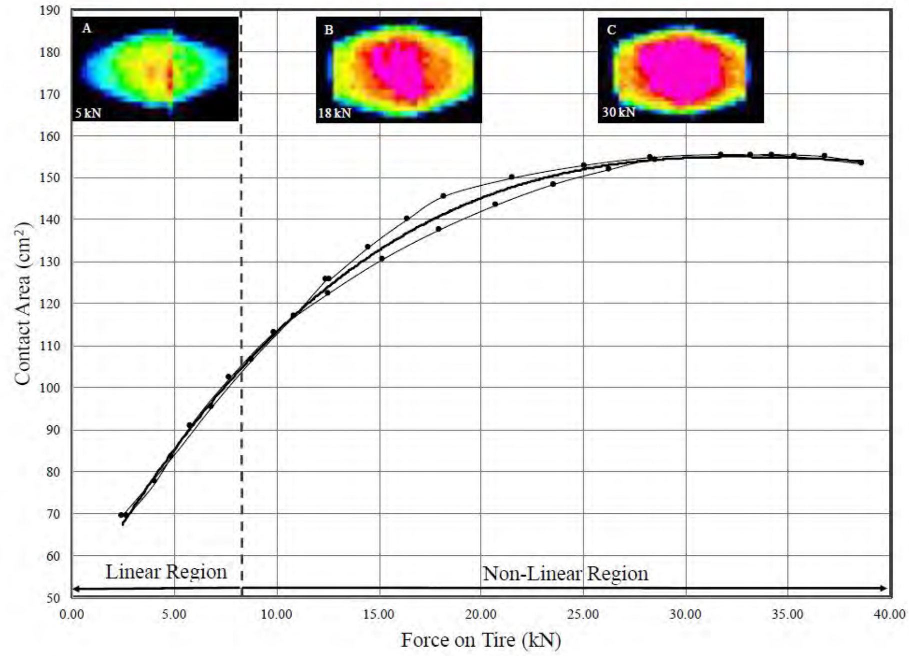

Figure 17: Contact area vs tyre load graph [5]

Test	Pavement structure	Demanded load (kN)	Measured load (kN)
1	500mm subgrade	2.7	2.10
		3.2	2.58
		3.7	2.98
		4.2	3.59
2	70mm base course 430mm subgrade	3.2	2.47
		3.7	2.96
		4.2	3.45
		4.7	3.93
3	140mm base course 360mm subgrade	4.2	3.52
		5.2	4.56
		6.2	5.54
		7.2	6.59

Table 2: Test plan

4. The APT was triggered by pressing the button and the tyre moved towards its start position without loading. The cameras were also triggered to start image capturing.

5. When the APT loading cycle began, the image frame number at that instant was recorded.

6. The loading curve was displayed on the computer and monitored throughout the cycle to ensure constant force was applied.

7. When the APT reached the end of its cycle, it was stopped by releasing the button. The frame number of the final image was recorded and the cameras were turned off.

8. Step 3-7 were repeated for other wheel loads.

4.5 Analysis Technique

4.5.1 Particle Image Velocimetry (PIV)

Particle image velocimetry (PIV) [24] allows observation of subsoil movement. Images are captured by camera every 0.9s. Each image is divided into a mesh of test patches, identifiable by pixel intensity from 0 to 255 depending on colour. To track the displacement of each test patch from one image to the next, a search zone size is specified. It represents the region within which the test patch is expected to lie. The correlation of pixel intensity between the test patch and each patch within the search zone is evaluated. The search patch which has the highest correlation is taken to be the new location. The magnitude and direction of the test patch displacement can then be obtained. This process is repeated for other images taken during each travel cycle. The precision of PIV is governed by equation (2), which increases with patch size but bigger patch means more computational effort is required. In my analysis, a patch size of 128×128 pixels was used, which corresponds to a precision of about 1/200th pixel. This translates to 4×10^{-4}mm in the object space.

$$\rho_{pixel} = \frac{0.6}{L} + \frac{150000}{L^8} \tag{2}$$

The PIV analysis was conducted in the image space of 2464×3264 pixels per frame. Therefore, it is necessary to convert the results into the object space of 180×240 mm. The control points on the window were used to determine the scale factor for conversion by measuring off the physical marker distance and also obtaining the pixel distance from image in Matlab. However, studies [24] reveal that the use of constant factor does not take into account of image distortion when the image is captured and would thus affect the accuracy of the analysis. Close range photogrammetry should be used instead to do the calibration.

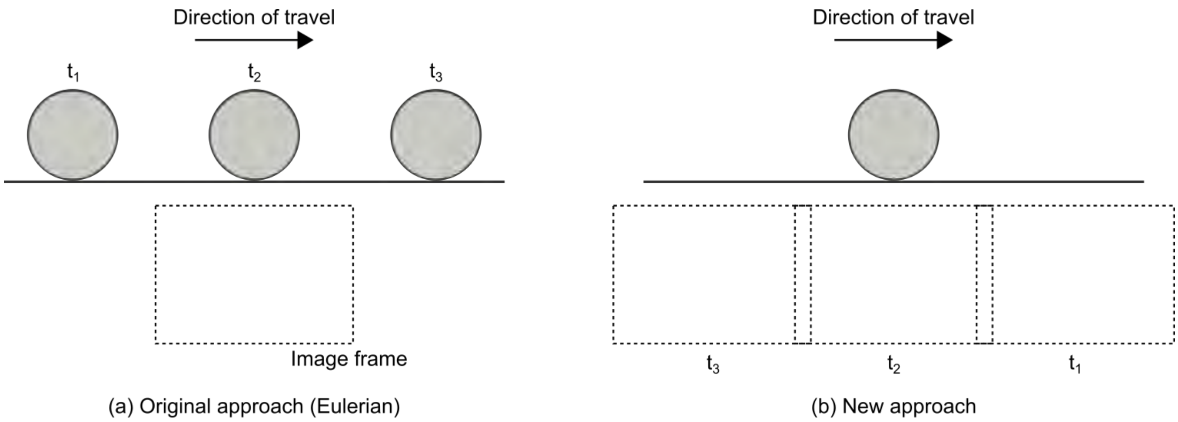

Figure 18: Soil tracking schematic

The quality of PIV analysis is dependent on the image quality. It is important to ensure even lighting in image by using LED light so that the soil grains are identifiable. The camera base plate was sprayed black to avoid any reflection onto the window, which would affect patch tracking. Also, sufficient image texture is required. Since the suggested value of artificial seeding ratio ASR is between 0.3 and 0.7 and the soil used for this study has $ASR_{subgrade} = 0.4681$ and $ASR_{base} = 0.5054$, seeding was not required [5].

4.5.2 Issues with Soil Tracking due to Wheel Movement

The project focuses on tracking soil movement under the wheel axis when it travels an incremental step. The experiment was designed such that the wheel moves while the camera remains stationary and captures images in an Eulerian frame of reference (Figure 18a). This means that the position of the wheel axis within the image frame changes with time. This setup implies that only the two consecutive frames captured at the instant when the wheel is directly in front of the camera should be used for analysis.

Preliminary test was conducted in the Michaelmas Term on a subgrade layer, with the wheel travelling at 25mm/s. The above approach was used to obtain the soil displacement vector field by using PIV results from two image frames only. It was found out that the wheel step, i.e. distance the wheel has moved in between frames, has a great influence on the experimental results. With a large wheel step, PIV fails to capture the details of the mechanism because each soil particle has undergone a series of motion in between frames. The soil displacement vector field for a large wheel step of 480mm is shown in Figure 19 to illustrate this issue. The mechanism is smeared out because it is a superposition of many finer mechanisms, originating from smaller wheel steps (Figure 20). Therefore, it is important to use a small wheel step to ensure that a fine mechanism can be captured.

In Lent Term, the APT speed was reduced to 5mm/s, corresponding to wheel step of 5mm between consecutive frames. A comparison between Figure 21 and Figure 19 shows the improvement. On the other hand, to make use of all the frames captured, an

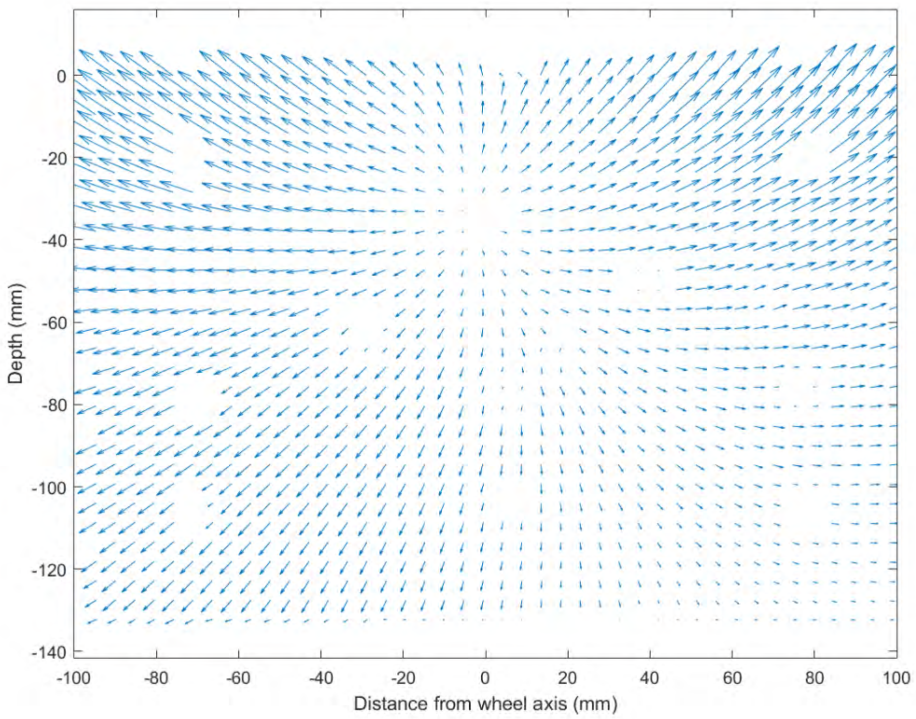

Figure 19: Soil displacement vector plot (single layered pavement, load = 3.59kN, wheel step = 480mm)

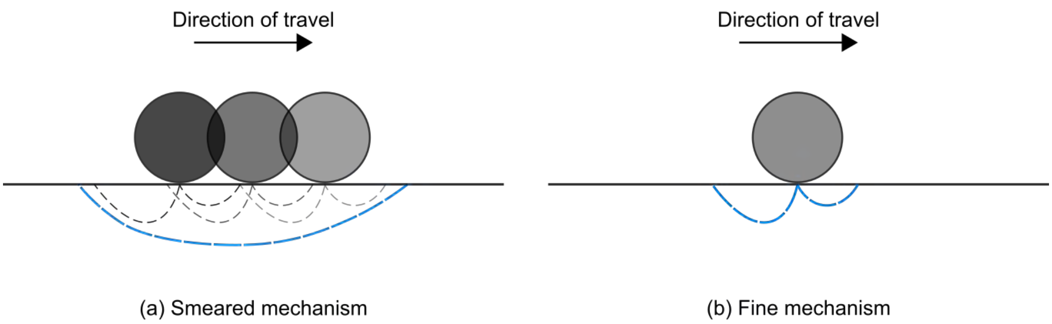

Figure 20: Influence of wheel step on captured deformation mechanism

alternative method was developed to analyse the soil displacement data. This method involves keeping the wheel stationary and having the image frames located at different positions (Figure 18b). As the frame rate, wheel speed and wheel start position are known, it is possible to equate the relative distance between the wheel axis and each frame as the wheel travels. Knowing this, the PIV displacement output from each frame can be mapped onto a new grid where the wheel is set stationary at zero position. A Matlab code was written to perform this mapping operation. As the frame rate is high when compared to the wheel speed, there is spatial overlapping between frames taken at adjacent time instant in the new grid as illustrated in the sketch. Therefore, any overlapping displacement values are averaged out, which help improve the accuracy. This method also increases the field of view so that the overall deformation mechanism can be observed.

4.5.3 Combining of Image Frames

Two rows of cameras were installed to capture the soil movement over a depth of 270mm. As the dimensions of each camera frame is about 240mm wide and 180mm deep, it is necessary to combine the two frames to obtain the overall deformation profile. The top and bottom frames overlap to a certain degree. The offset between the frames was determined using control points marked on the window. PIV analysis was done separately for each camera and then the results were combined by shifting the results by the offset value in object space.

5 Results and Discussion

Throughout this Section, the tyre moves in the positive horizontal direction.

5.1 Deformation Mechanism

5.1.1 Single Layered Pavement

The deformation mechanism for a single layered pavement is shown in Figure 21. The resultant displacement contour plot was used to help identify the flow zone boundaries when sketching the mechanism.

The sketched mechanism is compared with the mechanism for towed wheel proposed in previous research by Wong (Figure 6). It can be seen that for both, the front zone is wider than the rear. The major difference is that the rear zone in Wong's mechanism is much deeper and more skewed, which can be explained by their difference in wheel embedment. As dry sand was used in Wong's experiment, its strength and stiffness were derived primarily from friction between interlocking particles. This contrasts with the silty-sand used in this project, which gained its strength and stiffness from both friction and cohesion at optimum water content. Thus, much less wheel embedment and shoving motion were observed in my test, resulting in a slightly different mechanism. As mentioned in Section 3.5.1, the transition point is dependent on the direction of the resultant wheel force. It is reasonable that the transition point in the sketched mechanism is much closer to the wheel axis than Wong's because less horizontal force was needed to shove the soil pile in front of the wheel.

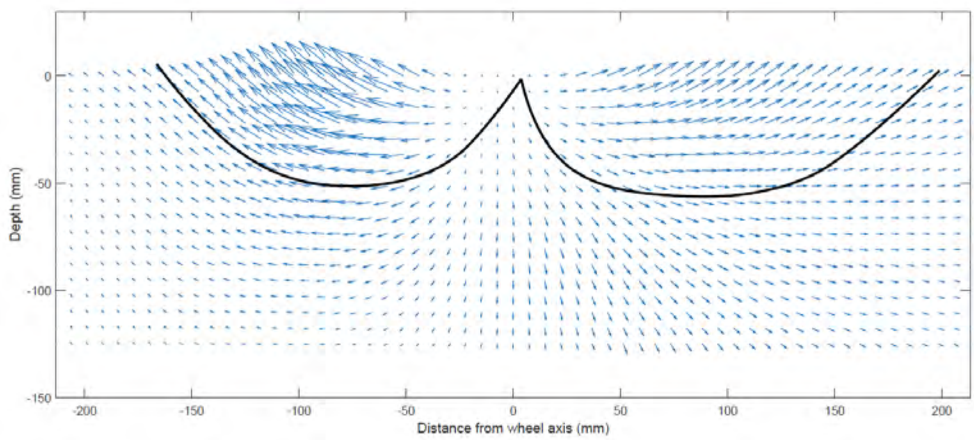

Figure 21: Soil displacement vector plot (single layered pavement, load = 3.59kN, wheel step = 5mm)

It is also worth comparing Figure 21 with Prandtl mechanism for inclined load (Figure 25). Stress fan rotation can be seen on both sides of the wheel and the transition point is close to the wheel. However, Prandtl mechanism predicts that the front flow zone would be smaller than the rear, which is different from the experimental results. This suggests that the soil deformation mechanism in my test is a combination of Wong's mechanism and the Prandtl mechanism.

The use of PIV reveals that tyre movement causes more horizontal than vertical displacement in general. In the horizontal direction, the displacement magnitude at the rear is greater although movement is concentrated within a smaller region (Figure 22). This suggests shear deformation is more significant at the rear, which is supported by the shear strain plot in Section 5.4 (Figure 31).

In the vertical displacement contour plot (Figure 22), it can be seen that there is little downward movement under the wheel. Upward movement can be seen in the two flow zones. In particular, the upheaval at the rear is significantly greater. During the test, the tyre was partially embedded into the soil, thus it had to push through the soil in order to traverse. This shoving action caused a soil pile to build up at the wheel front, which acted as a surcharge resisting the soil beneath from moving upwards (Figure 23). The small 10mm gap between the wheel and window meant that the soil pile formed was not in contact with the window. Therefore, the soil pile was not tracked by PIV but it reduced the upward movement of soil in front of the wheel. It also helped distribute soil movement over a greater distance.

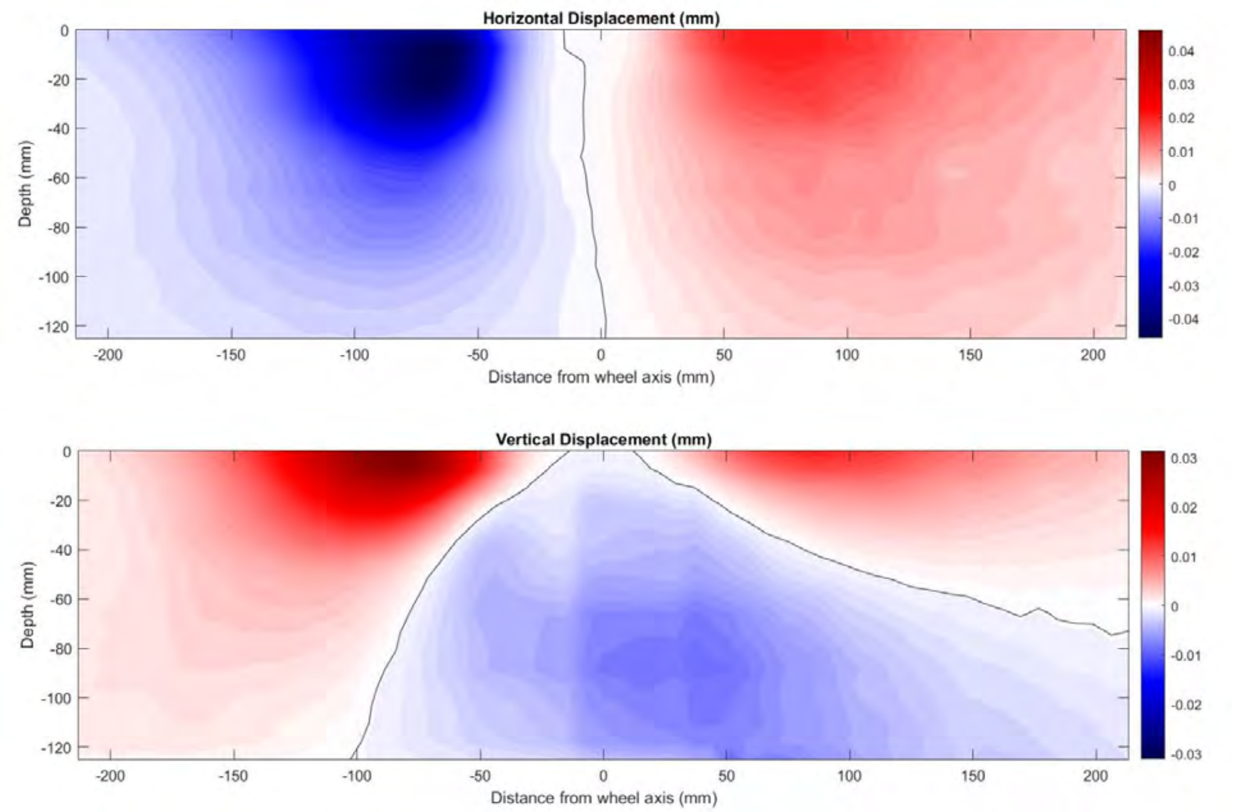

Figure 22: Displacement contour plots (single layered pavement, load = 3.59kN, wheel step = 5mm)

Figure 23: Formation of soil pile in front of the wheel

5.1.2 Two-Layered Pavement

There has not been much previous research on the deformation mechanism of subgrade in two-layered pavement. As the base course layer is stiff, the wheel does not embed into the surface when loading. Therefore, it is expected that soil would not deform in the same way as proposed by Wong in Section 3.5.1. Treating the narrow wheel contact patch as strip footing, the mechanism is compared with failure mechanism proposed by Prandtl for strip shallow foundations.

The base course helps distribute the wheel load over a greater area. Figure 24 shows the displacement vector field of soil particles. Note that soil movement in the base course is not considered in this analysis (see Section 5.7). Previous studies on multi-layered soil [10] proposed the load spread angle α to be $tan^{-1}0.5$ but it was also found that the value is dependent on soil properties. The outline of the load spreading mechanism is determined by identifying where discontinuity in soil displacement happens. It can be seen from the vector plot that load spreading is asymmetrical with α_1 and α_2 equal to 35° and 55°, which is reasonable due to the horizontal force imposed by the wheel during travel. The load spread angles suggest that a base course of 70mm thick would help increase the effective area of the wheel contact patch by threefold, thereby reducing the stress at the subgrade surface by threefold.

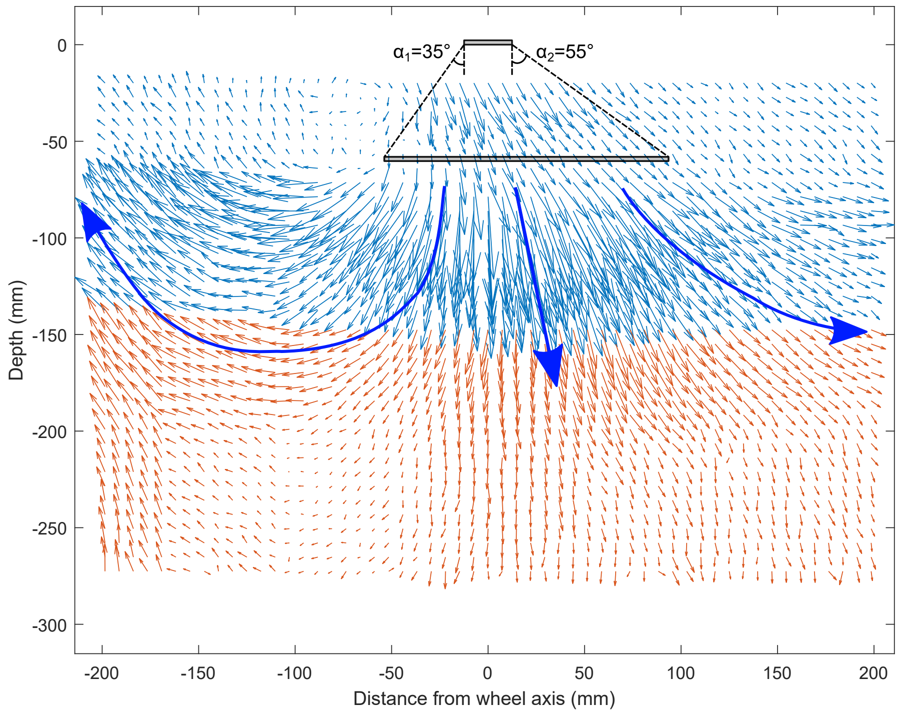

Figure 24: Soil displacement vector plot (two-layered pavement, 70mm base layer, load = 3.45kN)

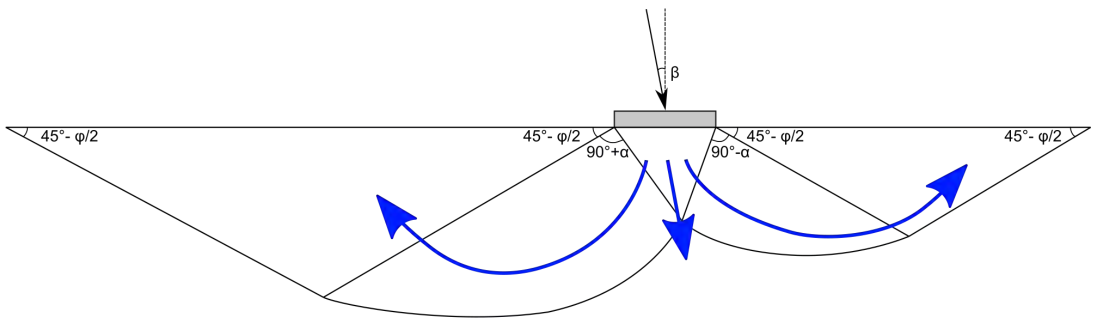

Figure 25: Prandtl failure mechanism for inclined load

As the wheel travels in horizontal direction, it is reasonable to compare the mechanism with the Prandtl failure mechanism for inclined load (Figure 25) [23]. As it is difficult to identify the exact flow zone boundaries from the vector plot, the outline of how the soil displacement direction changes with distance from the wheel axis is marked on the diagram. It can be seen that both mechanisms are skewed to the direction of travel. In Figure 24, the displacement vectors follow a spiral path at the rear of the wheel, which agrees with stress fan rotation proposed by Prandtl. To the front of the wheel, the direction of soil movement rotates slowly from vertical to horizontal but no upheaval can be seen. The rotation of stress is much less than expected. In fact, even though there is upward movement at the rear of the wheel, its magnitude is very small when compared to downward movement beneath the wheel as suggested in the vertical contour plot (Figure

26). This is probably because the base layer above is stiff and attenuates upward soil movement, in particular to a greater extent in the front zone. The region beneath the "load-spread" contact patch shows significant downward movement. Horizontal and vertical contour plots (Figure 26) show that soil deformation reduces to effectively zero over a subgrade thickness of about 130mm. This agrees with the Prandtl failure mechanism, which suggests there is no soil movement beyond stress fans and wedges. In general, stress blocks extend to a depth comparable to the foundation width, which is about 150mm for the "load-spread" contact patch in this test.

5.2 Sensitivity Analysis

A small wheel step of 5mm was initially used in doing PIV analysis for all 3 tests so that a fine deformation mechanism could be captured (Section 4.5.2) and all test results could be compared easily. However, displacement contour plots showed that for tests with base course, the displacements were very small. It was concerning that the displacements were too close to the precision of PIV (4×10^{-4}mm) and this would affect the validity of the experimental results. To verify the sensitivity of PIV at displacement range close to its precision, the images captured were re-sampled and re-analysed for the wheel cycle run on 140mm base layer at load = 3.52kN as it had the least amount of deformation. Re-sampling was done by extracting 1 frame in every 5 image frames to create a new batch, so that in subsequent PIV analysis, frame 1 would be compared with frame 5, frame 5 with frame 10 and so on. This increased the wheel step fourfold to 20mm but reduced the number of frames.

Although the vectors were more smeared out on the re-sampled vector plot, the deformation mechanism in subgrade could still be clearly identified. By linearity, it is expected that a fourfold increase in wheel step would lead to a fourfold increase in maximum soil displacement. Table 3 shows the a comparison between the original and re-sampled maximum displacements. The positive maximum horizontal displacement, whose magnitude was originally only 1.1 times the precision of the PIV, had a scale factor of 4.42. For other parameters which had greater magnitudes, their scale factors were very close to 4. This suggests that one should avoid having displacement comparable to the PIV precision. Therefore, all data collected from tests with base course layer were re-sampled to increase the step size to 20mm. As for the single layered pavement test, the wheel step remained unchanged at 5mm.

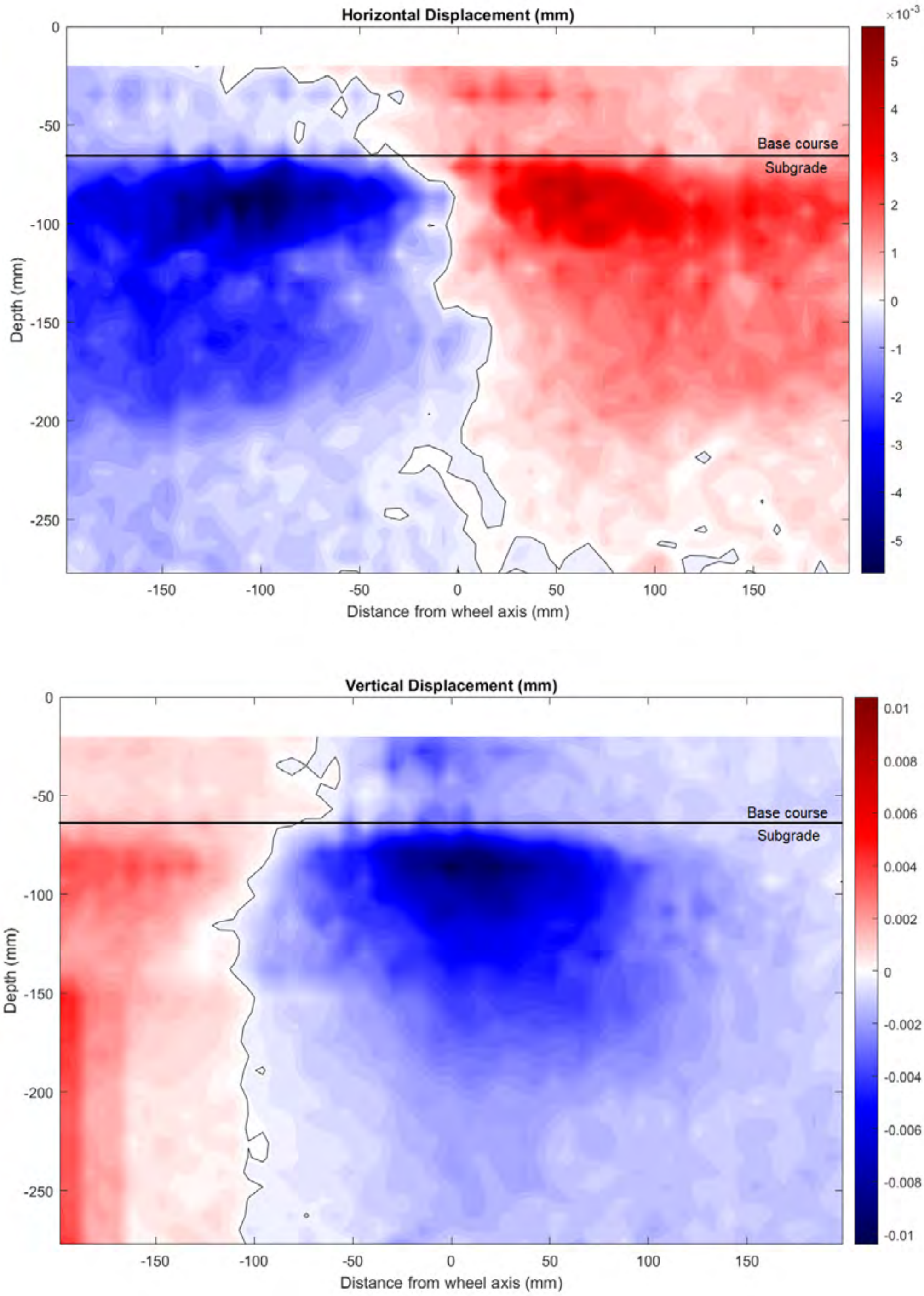

Figure 26: Displacement contour plots (two-layered pavement, 70mm base layer, load = 3.45kN, wheel step = 20mm)

Step (mm)	Horizontal (mm)		Vertical (mm)	
	negative	positive	negative	positive
5	-7.65×10^{-4}	4.52×10^{-4}	-1.3×10^{-3}	6.02×10^{-4}
20	-3.10×10^{-3}	2.00×10^{-3}	-5.0×10^{-3}	2.40×10^{-3}
Scale factor	4.05	4.42	3.85	3.99

Table 3: Maximum displacement for different wheel step sizes (two-layered pavement, 140mm base layer, load = 3.52kN)

5.3 Influence of loading

A pavement is subjected to different loads throughout its life cycle. Therefore, it is useful to understand the relationship between load and pavement deformation.

5.3.1 Magnitude of Soil Displacement

The absolute average displacement of soil patches is taken to be the characteristic parameter in this analysis. For single layered pavement, only soil particles within flow zones show sizeable movement. Thus, using all soil patches in the image frame to calculate the characteristic displacement would be misleading. Therefore, the average displacement for each load was calculated considering the soil patches within flow zones only. As for the tests on two-layered pavement structures, a similar approach was adopted and the soil movement in base course was neglected in the calculations.

As seen in Figure 27 and Figure 28, average displacement increases with wheel load for all three tests and it is possible to fit a linear trend line for each test. The linear relationship is as expected because the subgrade is frictional and obeys the Mohr Coulomb failure criterion. These trend lines suggest that there is a load below which no deformation would occur for each pavement structure when the line intercepts the horizontal axis. For the 3 pavement structures tested, it is estimated that this characteristic load would be 1.70kN. Due to the minimum loading range of the APT, it was not possible to verify this hypothesis. Since the weight of an average car is about 20kN (i.e. wheel load = 5kN), soil deformation is expected if it travels on the pavement structures constructed in this experiment.

For the single layered pavement plot (Figure 27), an outlier was ignored when fitting the trend line. Despite having the highest load of 3.59kN, the average displacement was significantly less than expected. This can be explained by how the experiment was carried out. During the test, wheel load was increased after running each cycle. As the wheel travelled on the subgrade layer, it shoved soil to the front. Soil piled up in front of the wheel as the number of cycles increased and this impeded any further wheel movement as it was no longer able to push the mass of soil. As a result, the pile of soil had to be removed manually and the top layer had to be re-compacted to restore a level surface before running passes again. The build-up of soil was not severe for the first three loads, thus cycles were run without the need to remove the soil pile. The wheel cycle at 3.59kN was run after re-compacting the subgrade, thus it is reasonable that the soil deformation was reduced. This reflects that the average soil displacement is also a function of the compaction effort. For the same compaction effort, it is expected that a linear relationship between displacement and load would hold. It was attempted to verify this assumption by running another pass at higher load, but severe piling up of soil meant that it was not possible.

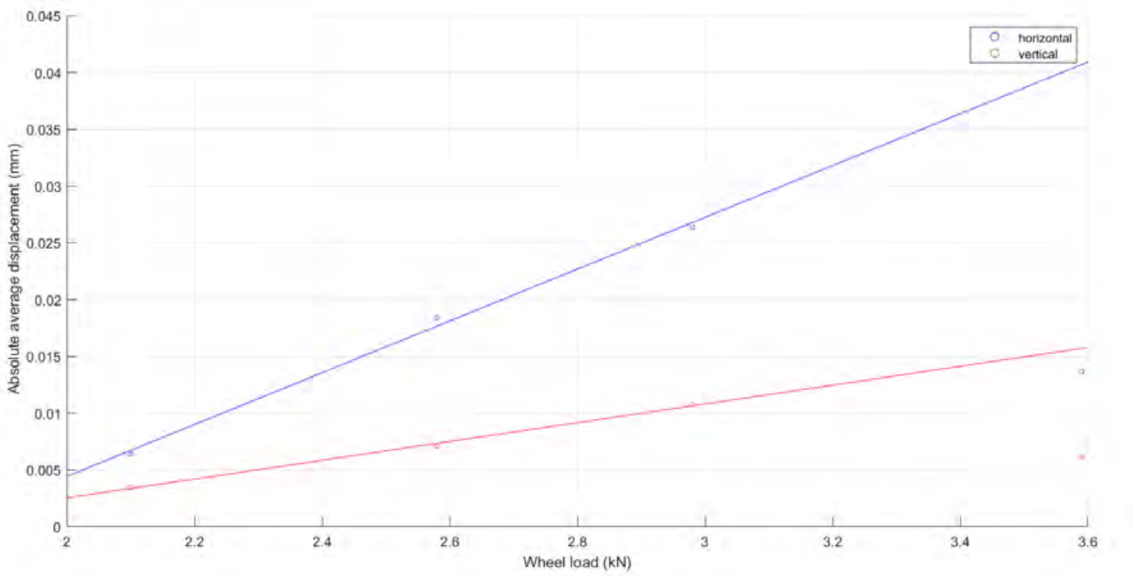

Figure 27: Absolute average displacement vs wheel load graph for single layered pavement test (wheel step = 5mm)

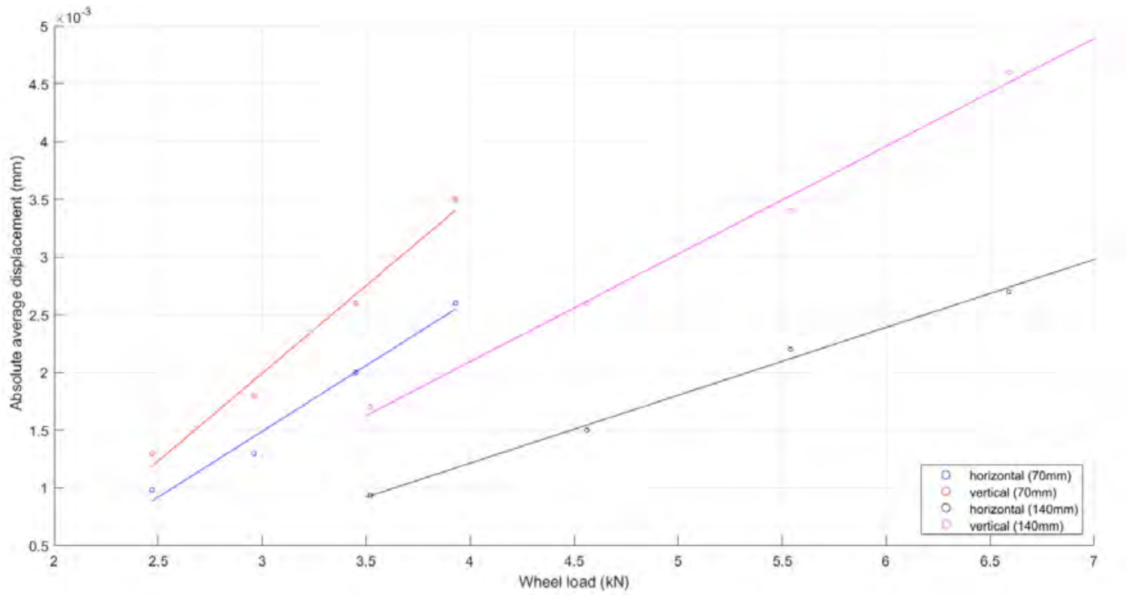

Figure 28: Absolute average displacement vs wheel load graph for two-layered pavement tests (wheel step = 20mm)

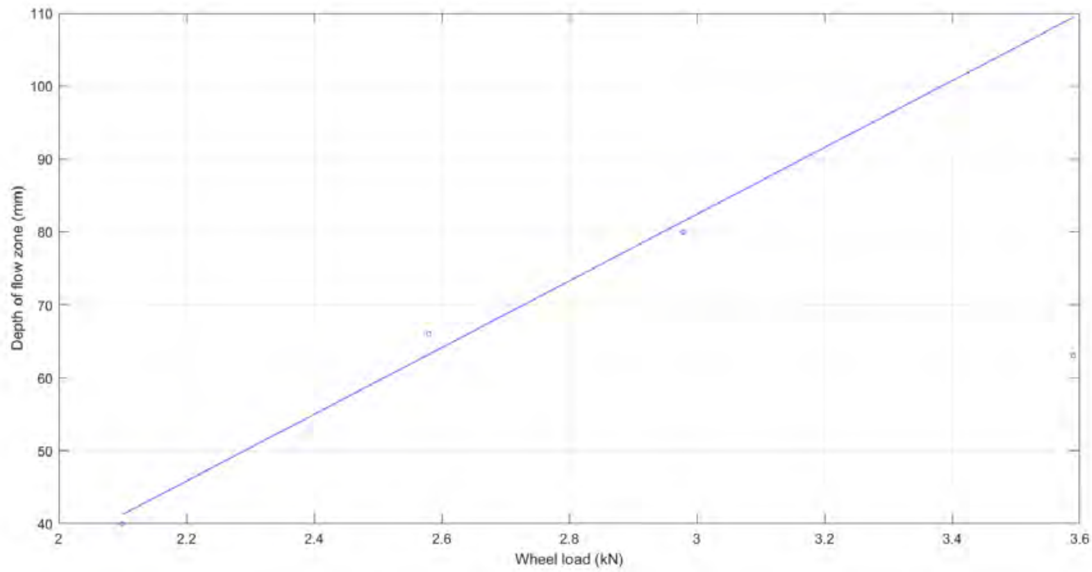

Figure 29: Flow zone thickness vs load graph (single layered pavement)

The formation of soil pile due to shoving limits the loads and number of cycles that can be run continuously on the subgrade. One possible way to solve this problem is to manually remove the soil pile as it builds up during wheel travel, but this would affect the subsoil movement mechanism because of the removal of surcharge. Another way would be to construct the pavement structure such that its surface slopes down as the tyre travels, so that the build up of soil pile would compensate the negative gradient. This method requires trial and error to determine what gradient works best.

5.3.2 Depth of flow zone

Understanding the influence of loads on flow zone size can help determine whether traffic causes disturbance to soil at depth. For a single layered pavement structure, the flow zone depth increases linearly with load (Figure 29). It can be seen that an increase in 1kN leads to an almost two times increase in flow zone thickness. This suggests that it is important for pavement engineers to estimate the maximum anticipated wheel load so as to design for the thickness of subgrade that would be affected by traffic.

In a two-layered pavement structure, it is difficult to identify the exact boundary of the flow zone from the displacement vector plot. Therefore, a plot is produced which shows how vertical displacement of soil particles varies with depth (Figure 30). The soil displacements were taken along the wheel axis where movements were significant. To facilitate comparison between different loads, the maximum vertical displacement along the line was normalised to unity. It can be seen that difference in loads does not affect the deformation behaviour much in the shallow region. However, the two sets of markers diverge with increasing depth. If the depth of flow zone is defined as the subgrade thickness to reduce the normalised displacement to 0.2, the flow zone depth for a wheel load of

2.47kN would be 80mm. An additional 20mm would be needed for a load of 3.93kN. This shows that with higher load, vertical displacement at depth is attenuated at a lower rate, i.e. it takes greater distance to dissipate stress. However, it should be noted that an increase of 20mm in flow zone depth for 1.5kN rise in load is very small. Thus, it is reasonable to treat the soil below about 100mm from top of the subgrade as undisturbed by wheel loads in design.

Note that the thickness of disturbed soil is dependent on how designers define the acceptable level of soil movement. The flow zone depth in the above analysis is determined arbitrarily but it is expected that the dependency between flow zone depth and wheel load would remain the same regardless of how it is defined as long as it is consistent.

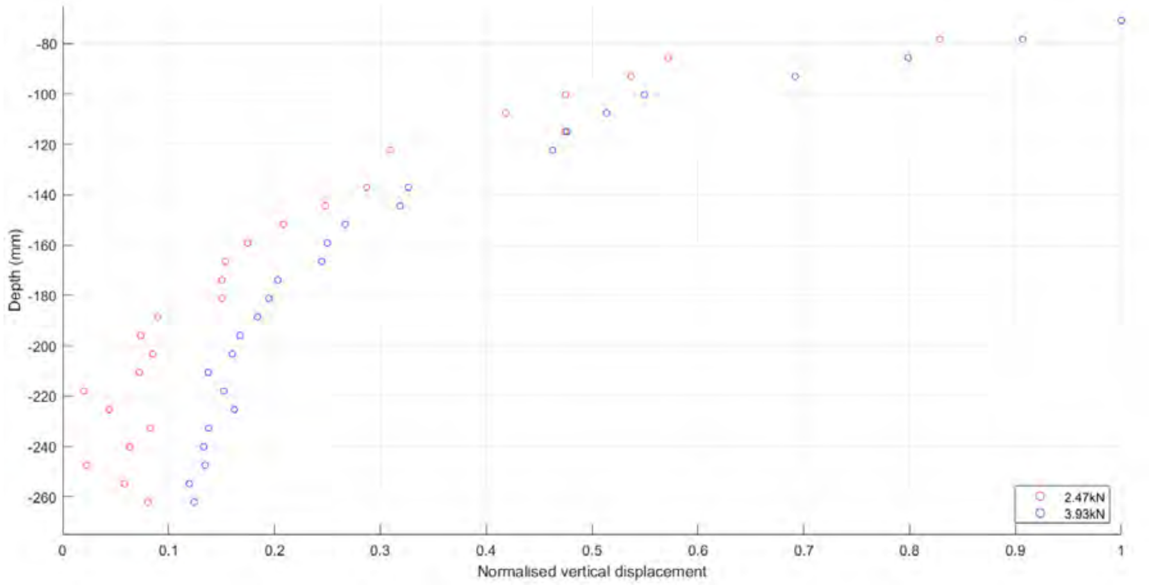

Figure 30: Depth vs vertical displacement graph (two-layered pavement, 70mm base)

5.4 Influence of travel repetition

The behaviour of soil changes with travel repetition in the single layered pavement test. Figure 31 shows 4 shear strain plots taken at different wheel cycles. It can be seen that the size of the front shear zone grows significantly from the 1st to the 3rd wheel pass, while the rear zone grows only moderately. A possible explanation would be that the area of shear zone increases with load because the wheel tends to embed deeper into the soil at high loads to increase contact area. As discussed in Section 5.1.1, deeper wheel embedment results in greater shear zone.

However, it can be seen that re-compaction in between the 3rd and the 4th cycle greatly reduced the size of front shear zone in subsequent travel. The suggests that repeated travel on pavement also influences the extent of shear deformation. This is probably because the soil state changes as the wheel moves through. The volumetric strain plot in Figure 32 shows that an incremental wheel step causes dilative movement in the flow zones and there is negligible volumetric contraction in the shallow region. This suggests that throughout each wheel pass, soil in the shallow region loosens up and becomes less dense. To verify this, a vertical displacement contour plot (Figure 33) is plotted for 1 wheel pass. It can been seen that the soil particles close to the surface indeed move upwards. At depth, there is minimal downward displacement. As the soil on the surface is no longer well-compacted, its shear strength reduces and the shear zone grows with the number of wheel passes.

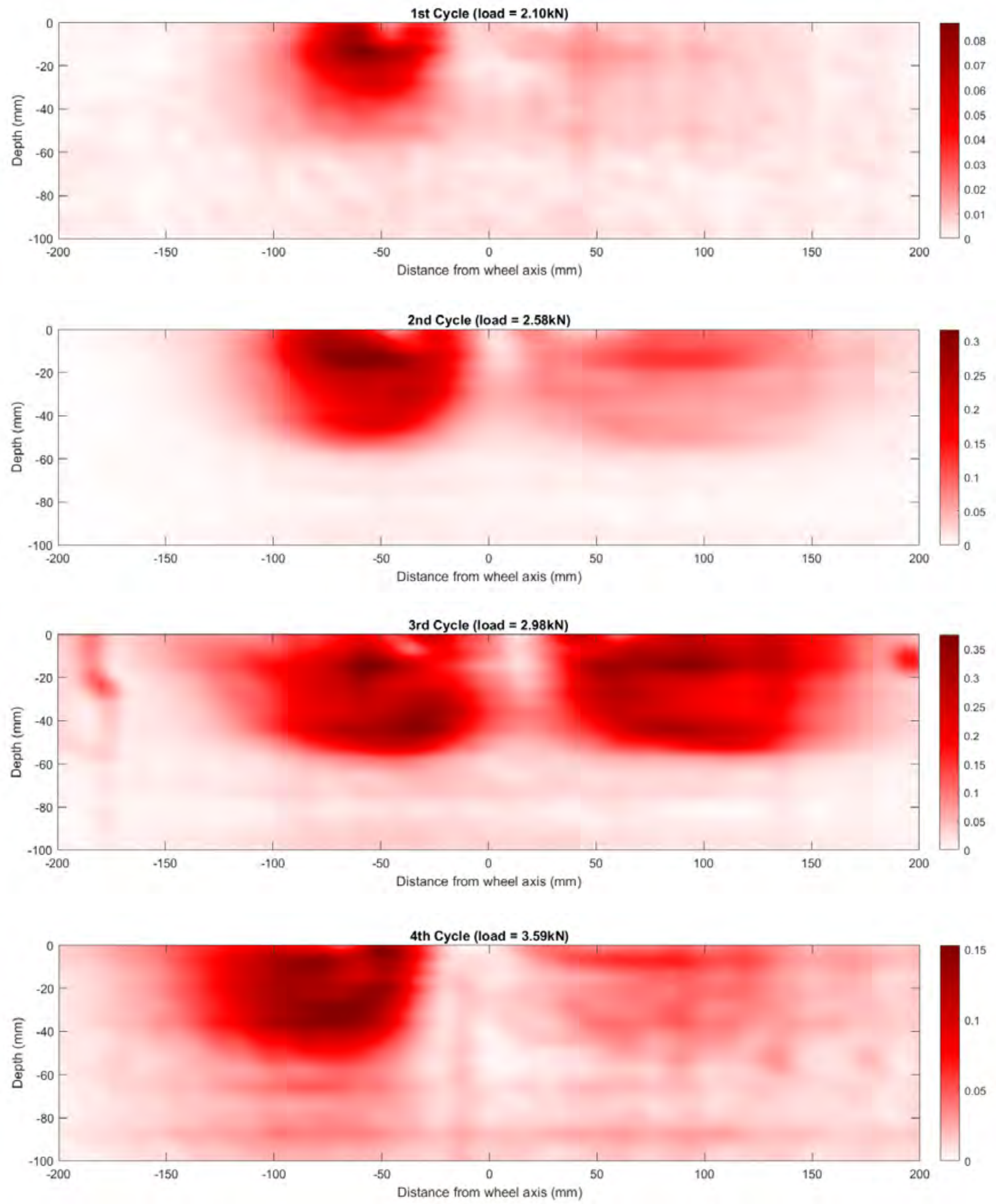

Figure 31: Shear strain plots for an incremental wheel step (single layered pavement, wheel step = 5mm)

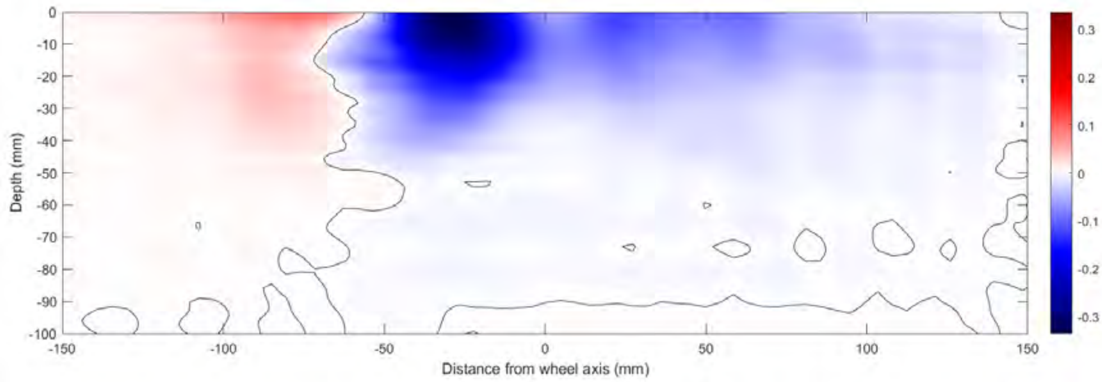

Figure 32: Volumetric strain plot for an incremental wheel step (single layered pavement, load = 2.58kN, wheel step = 5mm)

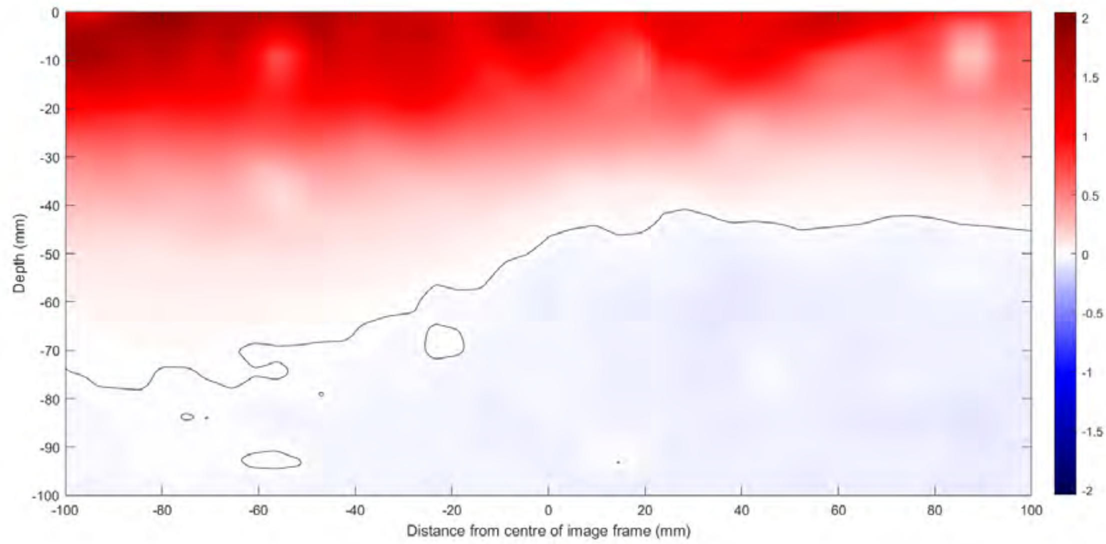

Figure 33: Vertical displacement contour plot for 1 wheel cycle (single layered pavement, load = 2.58kN)

5.5 Influence of Base Course Thickness

During the experiment, it was observed that the stiff base course greatly reduced the amount of rutting on the surface, which helped improve the serviceability of pavements. This Section focuses how the base course influences soil deformation in the subgrade layer.

As discussed in Section 5.1, the deformation mechanisms in the subgrade for single layered and two-layered pavements are significantly different. The overall deformation mechanism is the same for pavements with thin and thick base course. The displacement plots for the test with 140mm base course are attached in Appendix A for reference. A comparison between Figure 22 and Figure 26 shows that the base course mobilises soil movement over greater horizontal distance. With the thicker base course, the coloured patches in the contour plots are less localised. This is because the base course helps spread

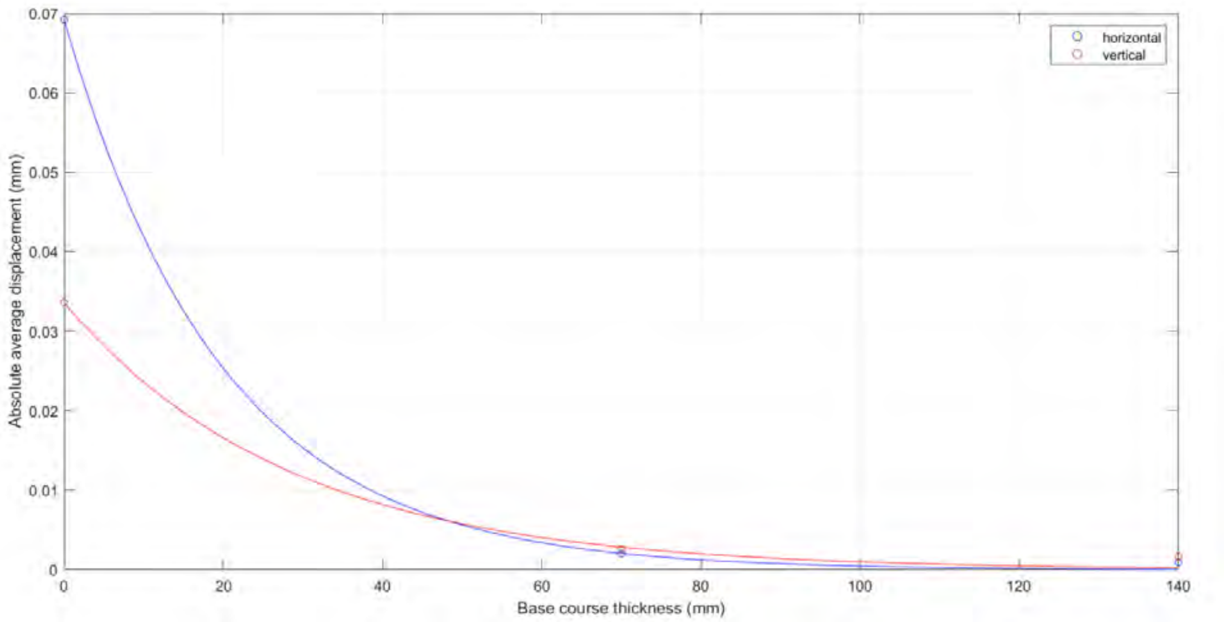

Figure 34: Absolute average soil displacement vs base course thickness graph (load = 3.50kN, step size = 20mm)

the load from the surface to a greater area in the subgrade. On the other hand, the base course reduces the amount of upheaval in the subgrade and this effect increases with the layer thickness, which can be clearly seen from the vector plots.

In a single layered pavement, horizontal displacement in the subgrade is generally greater than vertical displacement (Figure 27). But it is the opposite for pavements with base course layer (Figure 28). This suggests that base course attenuates shear deformation to a greater extent than nominal deformation in the wheel load direction. This is probably because there is friction at the interface between the subgrade and base course, which resists shear deformation in the subgrade. As for single layered pavement, the free surface on the subgrade is frictionless.

Figure 34 shows a plot of absolute average soil displacement against base course thickness, which seems to follow an exponential relationship. A base course thickness of 140mm helps reduce the horizontal displacement by 75 times and the vertical displacement in subgrade by 20 times. This shows that the base course is very effective in reducing deformation in the subgrade.

5.6 Soil Deformation in 1 wheel cycle

Previous sections have focused on soil deformation under an incremental wheel step. It is also useful to understand how soil deforms throughout an entire wheel pass by comparing two image frames taken before and after the cycle. Figure 35 and Figure 36 show how vertical soil displacement varies with depth. The soil displacement is taken at the centre of the image frame, which is midway along the wheel path. Results are then compared

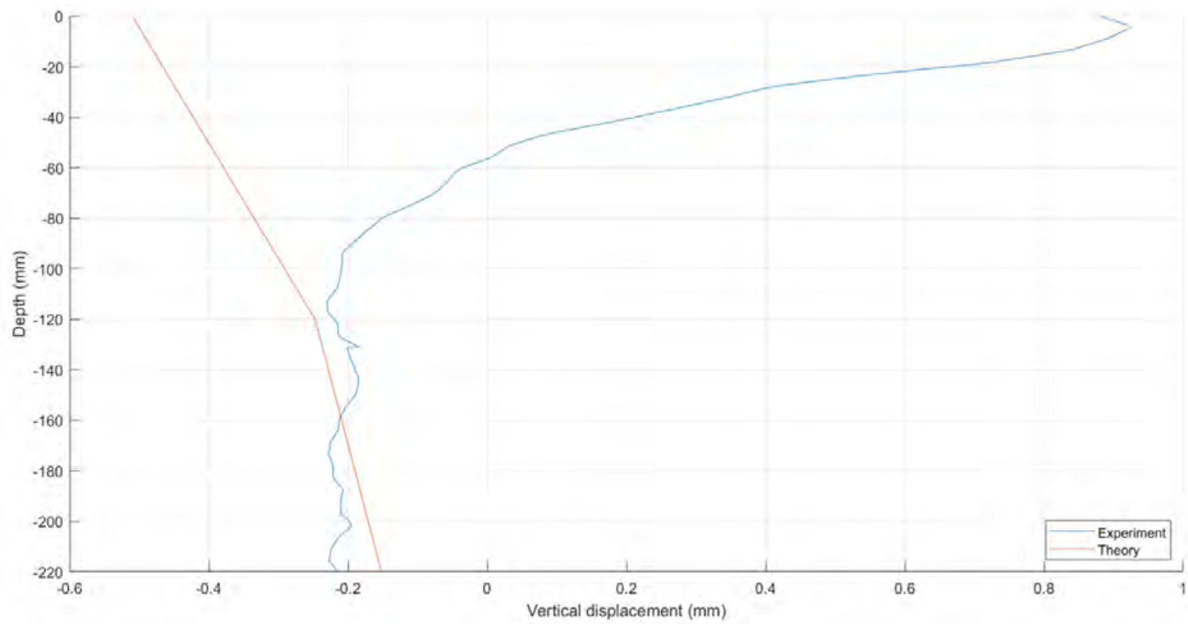

Figure 35: Depth vs vertical displacement graph for one wheel cycle (single layered pavement, load = 3.59kN)

with predictions from Burmister's equations (Section 3.1), which were derived based on layered elastic theory.

For the single layered pavement test (Figure 35), experimental results show that soil immediately below the surface moves upwards and dilates due to shear deformation during wheel travel. Yet, the theoretical curve suggests that all soil particles would settle downwards with a major compression zone at the top region. This is because in Burmister's derivation, the wheel is statically applying pressure onto the soil underneath, thus displacement along the wheel axis always points downwards. It does not take into account that the wheel is in fact in motion. This suggests that Burmister's equations are not suitable for characterising soil deformation in shallow region. Below a depth of 50mm, experimental displacement turns negative. It appears that soil displacement settles to a constant value of -0.2mm at depth, which is reasonably close to the theoretical prediction. This suggests that the dynamic effect of wheel load does not affect soil at depth and the layered elastic theory can be used to predict settlements.

Unlike single layered pavement, no upward movement is observed in the subgrade for the two-layered pavement test (Figure 36). This is probably because the base course helps dissipate any dynamic effect due to traffic. However, it can be seen that the magnitudes of experimental displacement are much less than that predicted by theory. Although the values do not match well, the use of layered elastic theory is conservative.

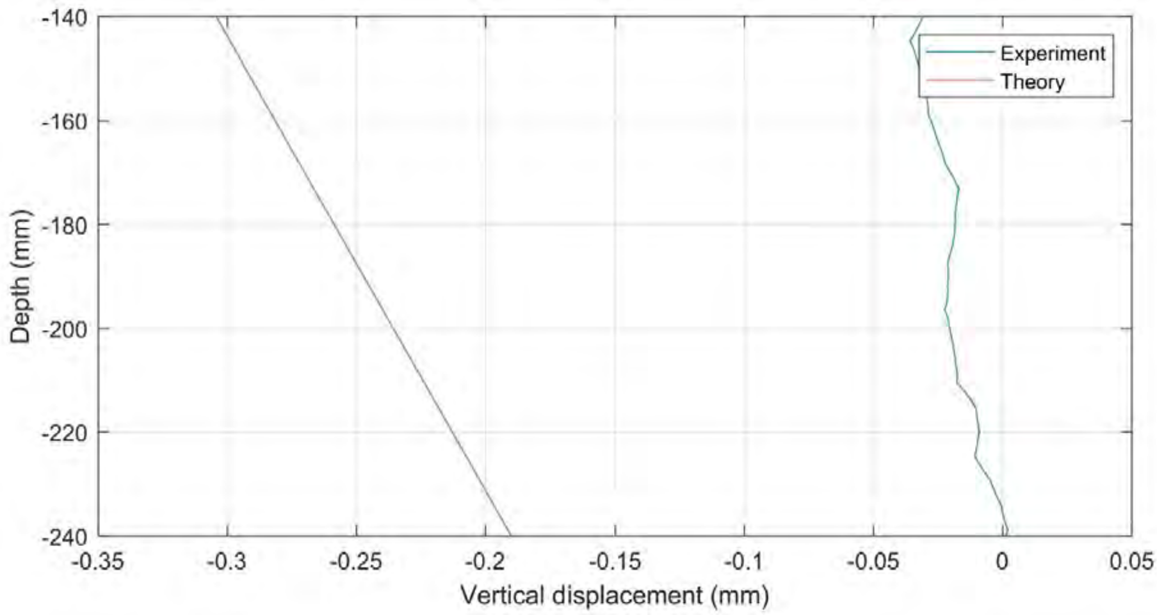

Figure 36: Depth vs vertical displacement graph for one wheel cycle (two-layered pavement, 140mm base, load = 6.59kN)

5.7 Issues with Tracking Base Layer Movement Using PIV

In general, results from PIV show that soil movement in the base course is less than that in the subgrade. Also, when comparing the results from the wheel pass at load of 3.50kN, the base course movement for the test with thicker base course (Figure 40) is significantly greater than that with thinner base course (Figure 24). These observations are different from what is expected. By looking at the images captured by the cameras (Figure 37), it can be deduced that the underestimation of base course movement is due to the silty paste on the window. The base course is made up of limestone aggregates with silty fines, which forms a paste when mixed with water to reach its optimum water content for compaction. The paste dries out over time and sticks on the window, which prevents the camera from capturing the aggregates movement behind it. PIV tracks soil movement by looking at how the position of each patch changes from one frame to another. As a large proportion of the patch is taken up by the silty paste, it difficult to perform tracking.

In order to verify this hypothesis, PIV was run on a small region which is covered by less paste (circled in red in Figure 37) to obtain soil displacement due to an incremental wheel step. Results are then compared with those from previous analysis using the entire image frame. As the size of the clean region is limited, the field of view of the contour plots is small. It can be seen from the plots (Figure 38 and Figure 39) that despite the deformation mechanism appearing to be roughly the same, the magnitudes of the displacement are different. The horizontal and vertical displacements tracked using the clean region are 33% and 10% greater than that using the whole image frame. This confirms the hypothesis that the silty paste affects PIV tracking. It is expected that this issue affects the 70mm base course test more because the paste is virtually blocking the entire view of the aggregates (Figure 37). This further explains why the base course displacement is smaller in the 70mm base course test than in the 140mm base course test despite having the same wheel load. Therefore, the data obtained for base course layer is neglected in the above discussion.

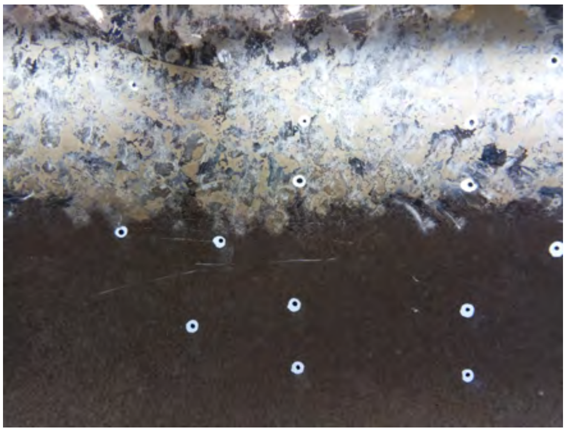

70mm base

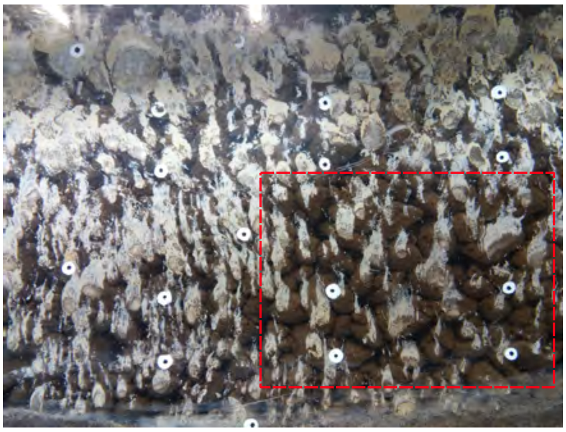

140mm base

Figure 37: Camera images

To solve this issue, one possible way would be to inject water into the side of the window to wash away the silty paste after finishing experimental setup. Time should be allowed for water to drain to the bottom of the pit before running any test. However, this may not be quite effective as the paste does not come off easily unless it is rubbed off by force. An alternative would be to place a thin metal plate to the side of the window when the base course layer is constructed. It acts as a barrier to prevent the wet paste from coming into contact with the window. After the paste dries out, the plate is removed so that it is possible to see the base course clearly from the window. As the base thickness is only up to 140mm, it is expected that not much force would be required to pull out the plate. To prevent any scratches on the window during compaction or plate removal, the plate should be wrapped with soft fabric.

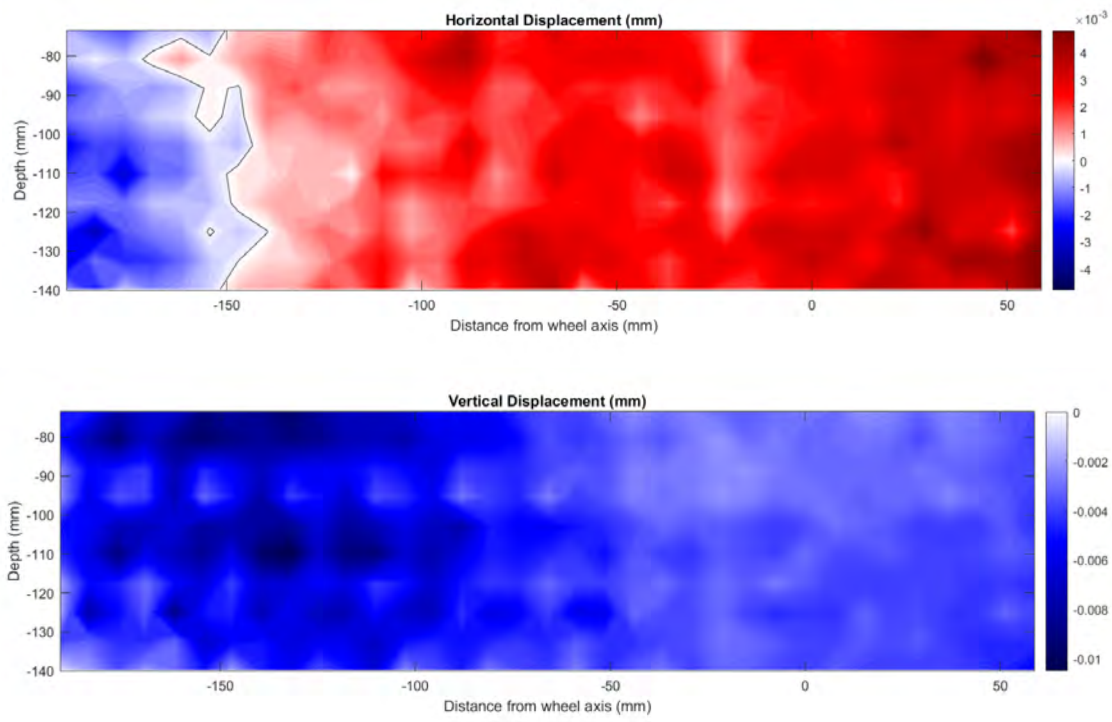

Figure 38: Displacement contour plots using small clean patch (two-layered pavement, 140mm base, load = 6.59kN)

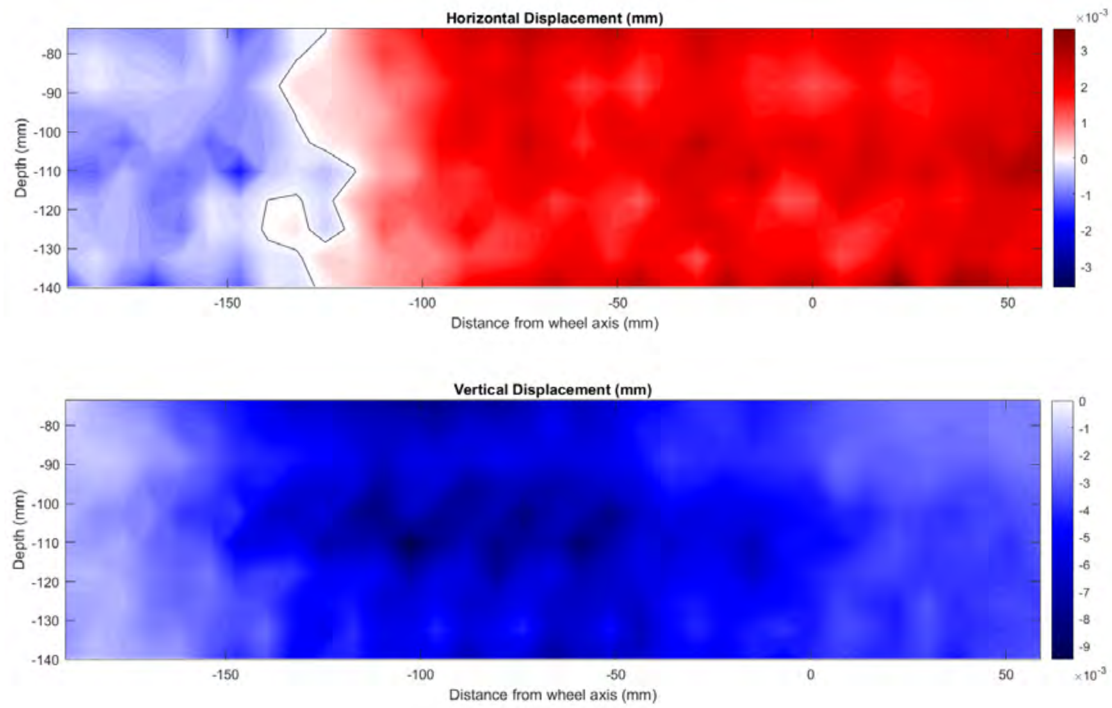

Figure 39: Displacement contour plots using entire image frame (two-layered pavement, 140mm base, load = 6.59kN)

6 Conclusions

In this project, in-path soil deformation under moving tyre in single layered and two-layered pavement structures was studied. Actual traffic conditions were physically modelled in the laboratory by running the APT on a pavement structure constructed in a pit. The following conclusions can be drawn from the experiment:

- The soil deformation mechanism in a single layered pavement structure (Figure 21) consists of two flow zones with the front wider than the rear. In general, the horizontal displacement is greater than the vertical displacement. The difference in soil displacement between the two flow zones can be explained by the soil pile formed in front of the wheel, which acts as a surcharge. For soft soil, the mechanism is similar to Wong's mechanism. As for soil with greater strength and stiffness, it is closer to the Prandtl mechanism for inclined load. The difference is due to change in wheel embedment.

- The base course in a two-layered pavement structure helps spread the wheel load and mobilise soil movement over a greater area in the subgrade. It also helps reduce upheaval in the flow zones. Friction at the base course/subgrade interface helps attenuate shear deformation to a great extent. On the whole, the base course is very effective in reducing deformation in the subgrade.

- For both pavement structures, average soil displacement increases linearly with load for the same amount of compaction effort. Depth of flow zone also increases with wheel load but to a lesser extent in a two-layered pavement structure.

- In a single-layered pavement, the front shear zone grows significantly with travel repetition while the rear zone grows only moderately. This is because soil in the shallow region undergoes shear deformation and dilation during each wheel pass, which reduces its shear strength.

- Layered elastic theory can be used to predict soil displacement at depth in single-layered pavement. However, it is not suitable for characterising soil deformation in shallow region because of the dynamic effects of the moving wheel load, which causes dilation near the surface. As for two-layered pavement, the theory overestimates soil displacement but results are conservative.

7 Future Work

Further study is required in order to develop a comprehensive understanding of pavement deformation under moving wheel load.

- A pavement withstands a large number of wheel cycles throughout its service life. In this project, only 1 cycle was run for each load to gain a fundamental understanding of how soil deforms and analysis was mainly focused on an incremental wheel step. More wheel cycles should be run on multi-layered pavement to understand soil behaviour in the long term. Analysis should be done on both the base course and the subgrade.
- Asphalt layer should be included in the future experimental setup. Although the thin layer does not provide much structural support, it is worth investigating how it affects the soil deformation mechanism. Fatigue cracking of asphalt layer is also another common cause of pavement failure that should be studied in detail.
- Vehicles on roads are either two-wheel-drive or four-wheel-drive, which operate differently from the towed wheel used in the experiment as torque is transmitted to each drive wheel. Therefore, the force acting on the soil would be different as well and this affects the soil deformation mechanism. It is necessary to change the design of the APT so that the tyre can operate as a drive wheel in future studies.
- The subgrade layer in a pavement normally consists of natural soil found in the environment. Only silt-sand was used in this project because it is difficult to prepare clay sample. In future experiments, clay should be used as well so that test results can be applied widely to pavements in different regions.
- Pressure measurement system should be incorporated into the future experimental setup. By measuring the direction and magnitude of the resultant wheel force, it is possible to come up with a more comprehensive model that relates wheel force to soil deformation mechanism.

8 Acknowledgements

I would like to thank my supervisor Dr Stuart Haigh for his guidance and support throughout the project. I would also like to thank Ms April Bowman for her invaluable help on the setup of the APT and advice on results analysis. I would also like to thank the technicians at the Schofield Centre, in particular Mr Mark Smith and Mr Kristian Pether for their help on experimental setup; research students Mr Geoff Eichhorn and Mr Chuhan Deng for their help on camera setup and PIV analysis.

References

[1] Tire tech: Load range/ply rating identification. https://www.tirerack.com/tires/tiretech/techpage.jsp?techid=55. Accessed: 10th May 2019.

[2] Budget 2018. Tech. rep., HM Treasury, 2018.

[3] Annual local authority road maintenance survey 2019. Tech. rep., Asphalt Industry Alliance, 2019.

[4] Borland, B. Bad roads a great danger to drivers. https://www.express.co.uk/news/uk/1065010/road-conditions-potholes-dangerous-driving-scotland. Accessed: 10th May 2019.

[5] Bowman. *Performance of Silty Sands and their Use in Flexible Airfield Pavement Design*. PhD thesis, University of Cambridge, 2018.

[6] Bowman, A. J., and Haigh, S. K. The Cambridge airfield pavement tester. *3rd European conference on physical modelling in geotechnics (EUROFUGE 2016)* (2016).

[7] Bowman, A. J., and Haigh, S. K. Subsurface deformation mechanisms beneath a flexible pavement using image correlation. *Géotechnique* (sep 2018), 1–11.

[8] Brown, S. F. Soil mechanics in pavement engineering. *Géotechnique 46*, 3 (sep 1996), 383–426.

[9] Brown, S. F. An introduction to asphalt pavement design in the UK. *Proceedings of the Institution of Civil Engineers - Transport 166*, 4 (aug 2013), 189–202.

[10] Burd, H. J., and Frydman, S. Bearing capacity of plane-strain footings on layered soils. *Canadian Geotechnical Journal 34*, 2 (apr 1997), 241–253.

[11] Burmister, D. M. The general theory of stresses and displacements in layered systems. i. *Journal of Applied Physics 16*, 2 (feb 1945), 89–94.

[12] Dareeju, B., Gallage, C., Ishikawa, T., and Dhanasekar, M. Effects of principal stress axis rotation on cyclic deformation characteristics of rail track subgrade materials. *Soils and Foundations 57*, 3 (jun 2017), 423–438.

[13] Hambleton, J., and Drescher, A. Modeling wheel-induced rutting in soils: Rolling. *J. Terramech. 46*, 2 (apr 2009), 35–47.

[14] Inam, A., Ishikawa, T., and Miura, S. Effect of principal stress axis rotation on cyclic plastic deformation characteristics of unsaturated base course material. *Soils and Foundations 52*, 3 (jun 2012), 465–480.

[15] Lekarp, F., and Dawson, A. Modelling permanent deformation behaviour of unbound granular materials. *Constr. Build. Mater. 12*, 1 (apr 1998), 9–18.

[16] Meyerhof, G. G. Some recent research on the bearing capacity of foundations. *Canadian Geotechnical Journal 1*, 1 (sep 1963), 16–26.

[17] MIURA, K., MIURA, S., and TOKI, S. Deformation behavior of anisotropic dense sand under principal stress axes rotation. *SOILS AND FOUNDATIONS 26*, 1 (1986), 36–52.

[18] Moreland, S., Skonieczny, K., and Wettergreen, D. Soil motion analysis system for examining wheel-soil shearing. *17th International conference for the society of terrain-vehicle systems* (2011).

[19] Nawaz, M. F., Bourrié, G., and Trolard, F. Soil compaction impact and modelling. a review. *Agron. Sustainable Dev. 33*, 2 (jan 2012), 291–309.

[20] Onafeko, O., and Reece, A. Soil stresses and deformations beneath rigid wheels. *Journal of Terramechanics 4*, 1 (jan 1967), 59–80.

[21] Saengprachatanarug, K., Ueno, M., Komiya, Y., and Taira, E. Measurement of soil deformation at the ground contact surface of a traveling wheel. *Engineering in Agriculture, Environment and Food 2*, 1 (2008), 14–23.

[22] Saengprachatanarug, K., Ueno, M., Komiya, Y., and Taira, E. Soil deformation beneath a wheel during travel repetition. *Eng. Agric. Environ. Food 3*, 3 (2010), 79–86.

[23] Van Baars, S. The inclination and shape factors for the bearing capacity of footings. *Soils and Foundations 54*, 5 (2014), 985–992.

[24] White, D., Take, W., and Bolton, M. Soil deformation measurement using particle image velocimetry (piv) and photogrammetry. *Geotechnique 53*, 7 (2003), 619–631.

[25] Wong, J. On the study of wheel-soil interaction. *Journal of Terramechanics 21*, 2 (jan 1984), 117–131.

[26] Wong, J.-Y. Behaviour of soil beneath rigid wheels. *J. Agric. Eng. Res. 12*, 4 (dec 1967), 257–269.

[27] Wong, J.-Y., and Reece, A. Prediction of rigid wheel performance based on the analysis of soil-wheel stresses part i. performance of driven rigid wheels. *Journal of Terramechanics 4*, 1 (jan 1967), 81–98.

A Supplementary Displacement Plots

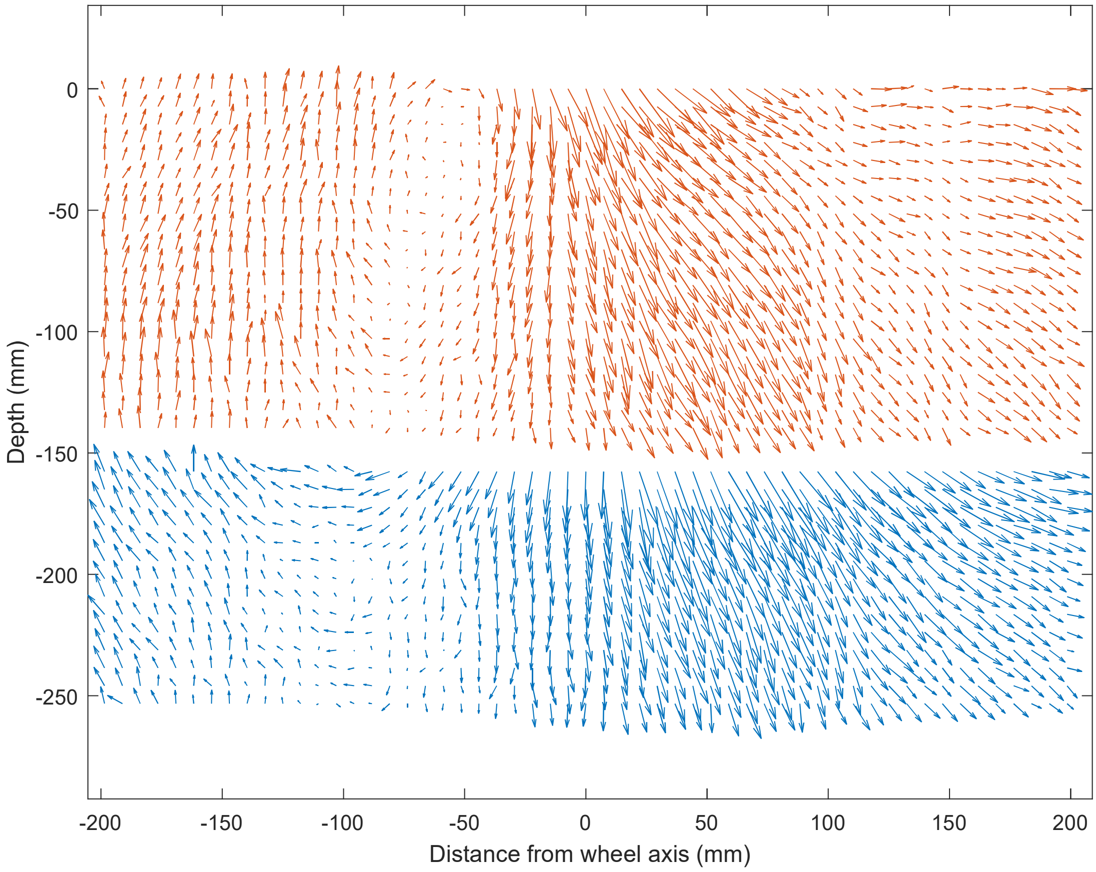

Figure 40: Displacement vector plots (two-layered pavement, 140mm base, load = 3.52kN, wheel step = 20mm)

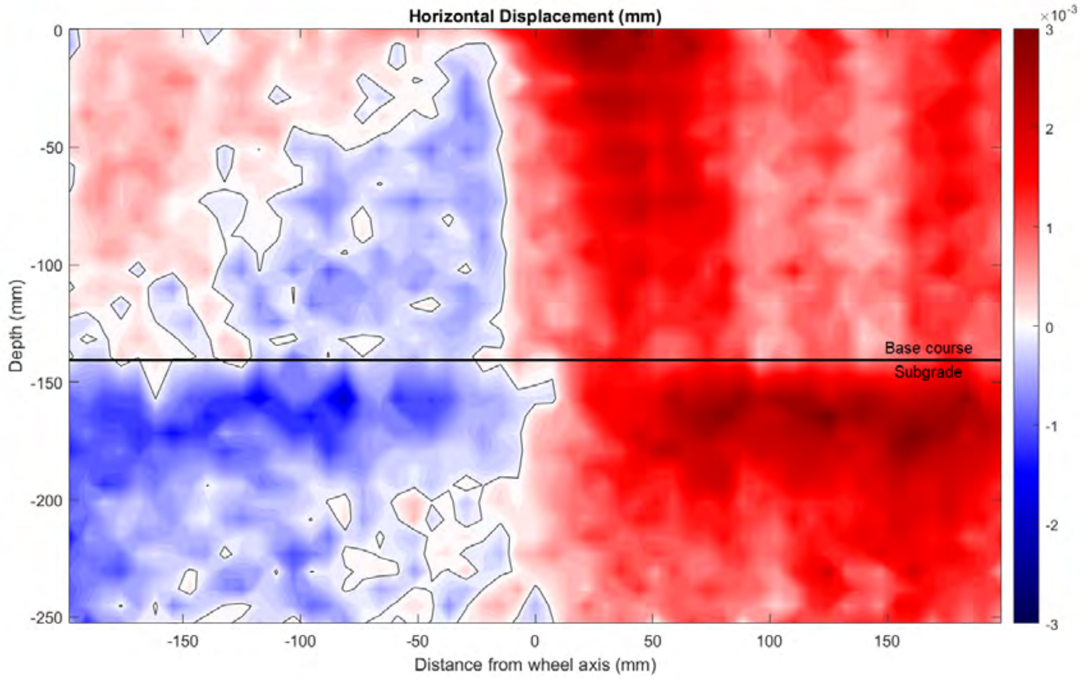

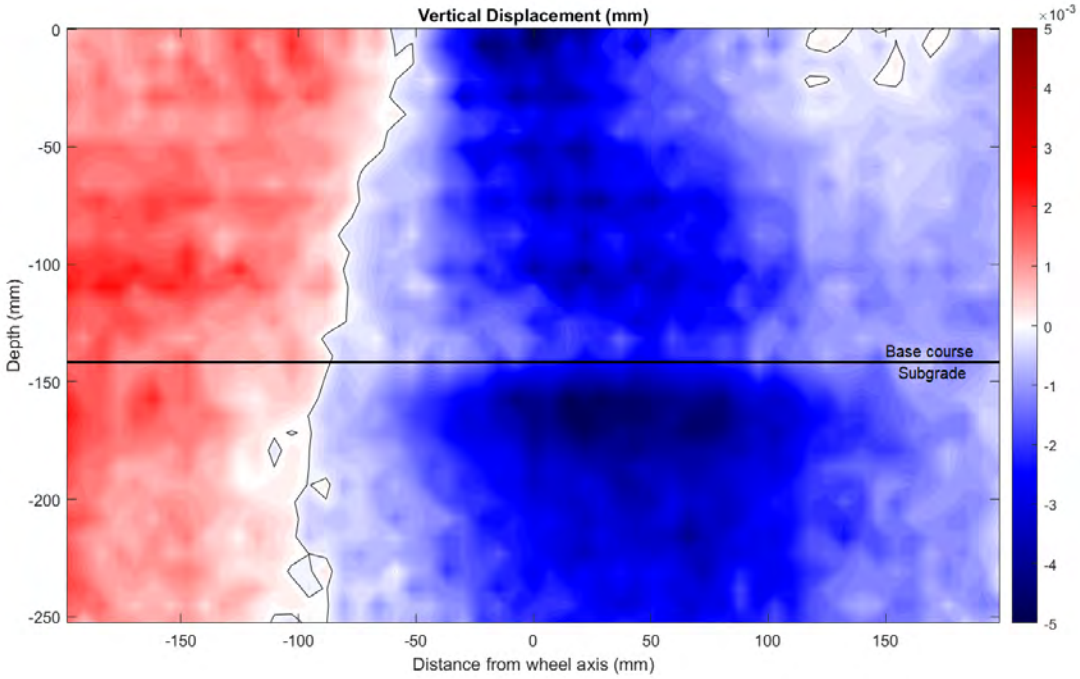

Figure 41: Displacement contour plots (two-layered pavement, 140mm base, load = 3.52kN, wheel step = 20mm)

B Risk Assessment Retrospective

On the whole, the risk assessment carried out at the start of the project was found to be suitable. The APT was moved into place for test by the technicians using appropriate lifting equipment and the pit opening was kept closed when not in use to prevent fall injury. The barrier to the equipment was also closed when the APT was in operation.

Nevertheless, some additional measures were taken to ensure health and safety throughout the experimental setup. As the base course material contains fine particulates, dust mask was worn during lifts and compaction. Gloves were also worn during the process. A dust extractor was used to remove dust generated in the laboratory environment. Mask and gloves were not used during construction of the subgrade layer as the soil was moist. On the other hand, the plate compactor was lifted into and out of the pit in pairs by following correct manual handling procedure. Help from the technicians was not needed as it was found that the load was manageable.

If a similar experiment is to be carried out in the future, the above measures should be added to the existing risk assessment document.